A simplified isotope dilution approach for the U-Pb dating of speleogenic and other low-[232]Th carbonates by multi-collector ICP-MS

Andrew J. Mason[1], Anton Vaks[1,a], Sebastian F. M. Breitenbach[2], John N. Hooker[1,b], Gideon M. Henderson[1]

[1]Department of Earth Sciences, University of Oxford, South Parks Road, Oxford, OX1 3AN, United Kingdom.
[2]Department of Geography and Environmental Sciences, Northumbria University, Ellison Place, Newcastle upon Tyne, NE1 8ST, United Kingdom.
[a]Present address: Geological Survey of Israel, 32 Yeshayahu Leibowitz Street, 9692100 Jerusalem, Israel.
[b]Present address: Department of Geosciences, Penn State University, 503 Deike Building, University Park, PA 16802, USA.

Correspondence to: Andrew J. Mason (Andrew.Mason@earth.ox.ac.uk)

Abstract. We describe a new method for the measurement of U/Pb ratios by isotope dilution multi-collector inductively coupled plasma mass spectrometry (MC-ICP-MS) for the dating of geologically young clean carbonates, particularly speleothems. The method is intended for materials containing little or no initial [232]Th. We illustrate and validate the method with four examples ranging from 0.57 Ma to 20 Ma old. The new method is capable of applying the [235]U-[207] and [238]U-[234]U-[206]Pb chronometers, common Pb and quantifiable residual [234]U/[238]U disequilibrium permitting. These provide an alternative to the more widely used[238]U-[206]Pb chronometer, which can be highly inaccurate for samples a few million years old, owing to uncertainties in the excess initial [234]U (hence, excess radiogenic [206]Pb) commonly observed in speleothems.

1 Introduction

Carbonates such as calcite and aragonite exist widely within the geological record, occurring as skeletal components of fossils such as corals, primary sedimentary deposits, secondary deposits such as speleothems, and as veins and fracture fillings. As such, carbonates have the capacity to capture a range of information about past sea level and climate, regional tectonics etc., and are of particular significance because they are often amenable to direct radiometric dating based on the decay of U and its various intermediate daughter products (Cheng et al., 1998; Edwards et al., 2003; Nuriel et al., 2012; Rasbury and Cole, 2009). Historically, this has been achieved mainly using [238]U-[234]U-[230]Th disequilibrium dating (e.g. (Scholz and Hoffmann, 2008 and refs. therein), or less commonly [235]U-[231]Pa disequilibrium dating (Cheng et al., 1998). These radiometric clocks are inherently limited to samples younger than the timescale over which the intermediate daughter used effectively returns to secular equilibrium; i.e. roughly 600,000 years for the [238]U-[234]U-[230]Th chronometer (Scholz and

Hoffmann, 2008). Uranium-lead dating, being based on the accumulation of stable radiogenic Pb does not suffer from this limitation, and has been applied for many decades to the dating of igneous and metamorphic accessory minerals (e.g. Heaman and Parrish, 1991) and has been utilised in a more restricted way to date comparatively old sedimentary carbonates (e.g. Moorbath et al., 1987; Rasbury et al., 1997; Wang et al., 1998). More recently, U-Pb dating has been adapted and applied to geologically young carbonates as a means of circumventing the c. 600 ka limit of the ^{238}U-^{234}U-^{230}Th chronometer, opening up far more of the geological record (Bajo et al., 2012; Cliff et al., 2010; Getty et al., 2001; Li et al., 2014; Pickering et al., 2010; Richards et al., 1998; Roberts et al., 2017; Vaks et al., 2020; Woodhead et al., 2006; Woodhead and Pickering, 2012). However, the U-Pb system remains comparatively underutilised in this regard and, given the variety of sample material available and differences in laboratory set-up, it is unlikely that any implementation of the U-Pb system will be universally applicable. To this end, we document in detail a novel protocol for the U-Pb dating of carbonates by isotope dilution MC-ICP-MS recently used in a study of Siberian permafrost (Vaks et al., 2020).

2 Overview of the U-(Th)-Pb system and the motivation for a new method

The U-Th-Pb system is based on the twin decay chains of ^{238}U to ^{206}Pb and ^{235}U to ^{207}Pb, plus the decay chain of ^{232}Th to ^{208}Pb, and unradiogenic ^{204}Pb. The latter decay chain is not of direct relevance here as we are only considering systems that have sufficiently low ^{232}Th that ^{208}Pb can also be treated as unradiogenic. Owing to the insolubility of Th in many aqueous systems, many carbonates approximate to a ^{232}Th-free system (e.g. Thomas et al., 2012; Vaks et al., 2013b).

Most previous U-Pb work on carbonates has focused on the ^{238}U-^{206}Pb system taking either a traditional isotope-dilution solution-based approach where the samples are spiked with an isotopic tracer, dissolved, and then the U and Pb purified for analysis on a multi-collector MS, or have utilised *in situ* laser ablation analysis (e.g. Getty et al., 2001; Pickering et al., 2010; Roberts et al., 2017; Woodhead et al., 2006). We initially pursued the former route (Mason et al., 2013) as it offers better precision, e.g. < 0.1% uncertainty versus c. 0.6% or more by laser ablation on the ^{234}U/^{238}U ratio and < 1 % by isotope dilution versus 5-10% by laser ablation on the ^{238}U/^{206}Pb ratio, as well as the ability to date younger material with lower U and Pb concentrations (Cheng et al., 2013; Lin et al., 2017; Roberts et al., 2017; Spooner et al., 2016; Woodhead et al., 2006; Woodhead and Petrus, 2019). However, setting-up and maintaining low-Pb blank anion exchange chromatography involves considerable effort, and its application generally requires an additional layer of reconnaissance analyses to target samples or parts of samples that are sufficiently radiogenic to date. Having a simplified procedure that minimises the opportunity to introduce Pb blank, that does not require reconnaissance U-Pb characterisation, and maintains acceptable precision, was a significant motivation for developing a new method.

A caveat in U-Pb dating is that calculated U-Pb ages can strongly depend on the assumptions made regarding the initial state of the decay chains, especially initial ^{234}U/^{238}U, ^{230}Th/^{238}U and ^{231}Pa/^{235}U ratios (Ludwig, 1977). For carbonates precipitated from fresh or sea waters, initial ^{230}Th and ^{231}Pa are likely to have been near absent owing to their insolubility in aqueous

65 systems (Cheng et al., 1998; Edwards et al., 2003) and, thus, in practice do not present a major source of age uncertainty. However, initial ^{234}U can be strongly enriched with initial ^{234}U/^{238}U ratios as high as 7 to 12 times equilibrium known (Kronfeld et al., 1994; Plagnes et al., 2002; Vaks et al., 2013b). If unaccounted for, the initial ^{234}U excess could lead to ^{238}U-^{206}Pb age inaccuracies of upwards of 2 Ma. For (typically <2 Ma old) samples where the initial ^{234}U disequilibrium has not yet completely decayed, the initial ^{234}U/^{238}U ratio can be calculated from the measured ^{234}U/^{238}U ratio as part of the age

70 calculation (here termed the ^{238}U-^{234}U-^{206}Pb chronometer), avoiding such inaccuracies. However, for older material, the initial ^{234}U/^{238}U ratio must be assumed in the age calculation (here termed the ^{238}U-^{206}Pb chronometer), potentially leading to significant inaccuracies in assessed ages. Where ages extend beyond the limit of the ^{238}U-^{234}U-^{206}Pb method, particularly where there is evidence for large variability in initial ^{234}U/^{238}U ratios, the ^{235}U-^{207}Pb chronometer could prove a powerful alternative dating tool. Such a situation was found in speleothems from Siberian caves (Vaks et al., 2020), which provided an

75 additional motivation for developing the dating approach presented here. We pursue a solution-based method over laser ablation in order to maximise the range of the ^{238}U-^{234}U-^{206}Pb chronometer by obtaining precise ^{234}U/^{238}U measurements and, because it represents a better prospect for detecting the tiny quantities of radiogenic ^{207}Pb necessary to apply the ^{235}U-^{207}Pb chronometer to samples a few Ma old.

80 A second caveat in U-Pb dating is that carbonates often contain an appreciable amount of initial (common) Pb that must be accounted for, usually requiring some form of isochron technique, though the choice of isochron used varies widely (e.g. Mason et al., 2013; Pickering et al., 2010; Woodhead et al., 2006). One approach (e.g. Roberts et al., 2017) is to use the intersection of an isochron in ^{238}U/^{206}Pb – ^{207}Pb/^{206}Pb (Tera-Wasserburg) space with concordia to determine the ^{238}U/radiogenic^{206}Pb ratio and, by extension, the age. However, this approach precludes an independent assessment of the

85 ^{235}U/radiogenic^{207}Pb ratio, inhibiting the use of the ^{235}U-^{207}Pb chronometer. An arguably better approach is to use isochrons based around unradiogenic ^{204}Pb (e.g. Rasbury and Cole, 2009). This allows for independent correction of common ^{206}Pb and common ^{207}Pb permitting the usage of both the ^{238}U-^{206}Pb and ^{235}U-^{207}Pb systems, though using ^{204}Pb has the practical drawbacks of it being a low-abundance isotope and suffering an isobaric interference on ICP systems from instrumental Hg. However, in effectively ^{232}Th-free samples, the much more abundant ^{208}Pb can be used in place of ^{204}Pb as the unradiogenic

90 Pb isotope (e.g. Mason et al., 2013). Implementing a streamlined ^{208}Pb-based approach, which obviously requires that ^{208}Pb be measured, was a further motivation for the development work presented here.

In summary, the objective of the present work is to present a new isotope-dilute based method that seeks to streamline the sample preparation, particularly with regard to analysing blank-sensitive Pb/Pb and U/Pb ratios and, which, allows a ^{208}Pb-

based approach to common Pb correction, such that the ^{238}U-^{234}U-^{206}Pb and ^{235}U-^{207}Pb chronometers can both be utilised, where the nature of the sample permits.

3 Protocol description

3.1 Reagents/Equipment

Analyses were performed by isotope dilution using a mixed ^{236}U-^{204}Pb-^{230}Th spike dissolved in c. 2 M HNO$_3$ (Mason et al., 2013) using a first generation Nu Plasma MC-ICP-MS (Belshaw et al., 1998) fitted with 'B-type' Ni cones. Sample introduction was via a DSN100 (Nu Instruments) desolvator using either a c. 50 µL min^{-1} or 75 µL min^{-1} self-aspirating PFA nebuliser (ESI). Sample preparation and analysis required the following reagents and consumables:

- 18.2 MΩ.cm water
- Quartz-distilled 10 M HCl and dilutions of this
- Quartz-distilled 16 M HNO$_3$ and dilutions of this
- Reagent grade 16 M HNO$_3$
- Bio-Rad AG-1 X8 anion exchange resin (or equivalent)
- 15 ml polypropylene bottles acid cleaned for ~ 1 week in 1-2 M distilled HNO$_3$, then rinsed thoroughly with 18.2 MΩ.cm water
- 22 ml or 27 ml PFA vials acid cleaned in hot, concentrated reagent grade HNO$_3$ for ~1 week, then refluxed in distilled 10 M HCl for at least 24 hours, and thoroughly rinsed with 18.2 MΩ.cm water after each acid stage
- 2 ml Bio-Rad polyprep columns (or equivalent) acid cleaned for ~1 week in 1-2 M distilled HNO$_3$, then rinsed thoroughly with 18.2 MΩ.cm water
- CRM145 (New Brunswick Laboratory) natural U, or equivalent U isotopic reference material.
- Single element Tl standard

3.2 U-Pb measurements

The U-Pb preparation protocol and analytical protocol is summarised in flow chart form in Figs. 1 and 2 respectively. Subsamples were cut from carbonate samples using a small diamond circular saw and transferred to acid-cleaned 15 ml polypropylene bottles. These subsamples were then sonicated repeatedly in 18.2 MΩ.cm water until no suspended particles were visible, rinsing between each wash. The subsamples were then twice acid cleaned for a few minutes in distilled 2 % HNO$_3$ with sonication to remove any residual dirt and surface contamination. Following each wash, the samples were thoroughly rinsed with 18.2 MΩ.cm water and sonicated to ensure removal of any residual acid and dislodged surface material. Each acid wash was removed before the acid was consumed, to prevent adsorption of dissolved ions back on to the surface of the sample. Subsamples need to be sufficiently large that c. 10 mg survives acid cleaning. We used initial masses

125 of a few hundred milligrams for ease of handling during cleaning, but this can be reduced where sample material is limited. Cleaned subsamples are then stored until the day of analysis. Because of the minimal sample preparation required, redundant subsamples can be cut and cleaned with little extra effort. This allows the real-time targeting of radiogenic material as it is identified within an analytical session, without the need for prior reconnaissance characterisation of the U-Pb system.
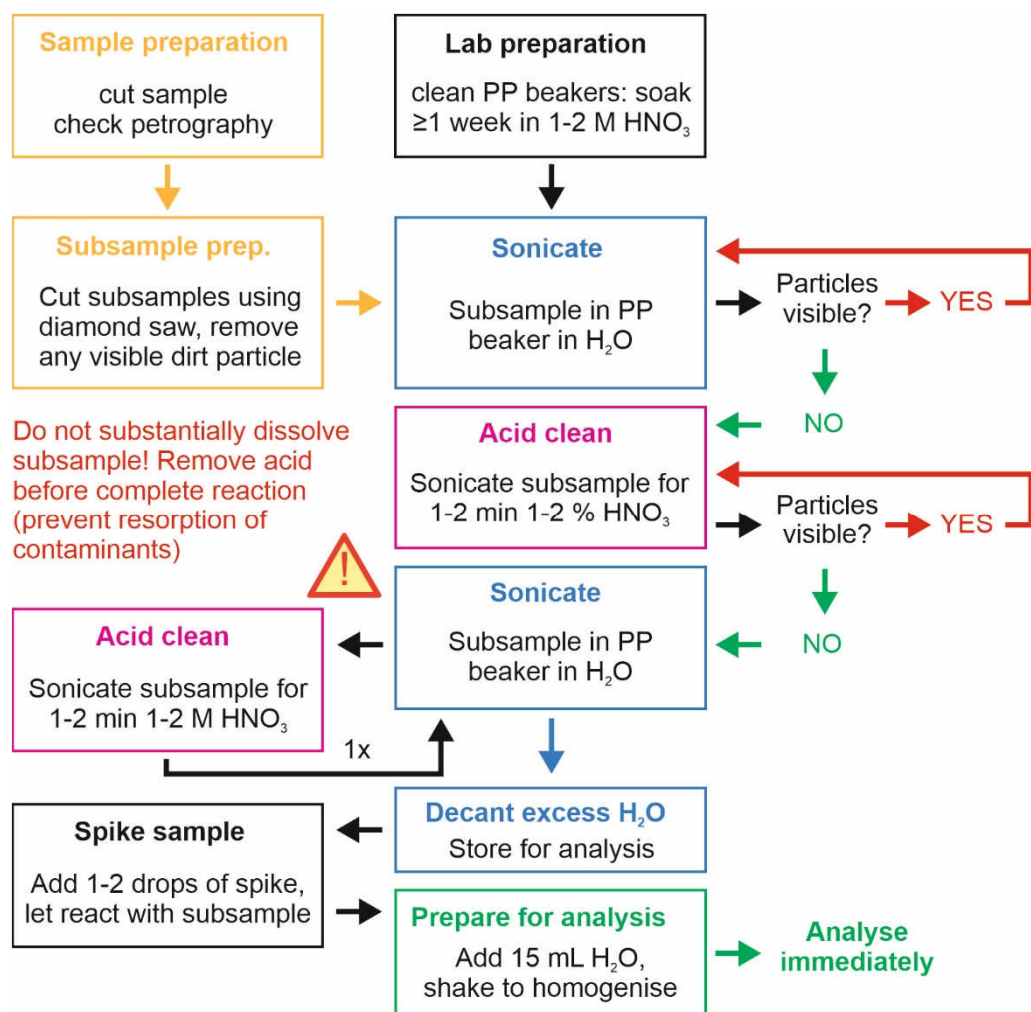
130

Figure 1: flow chart showing sample preparation protocol. The spike is a mixed ^{236}U-^{230}Th-^{204}Pb tracer in c. 2M HNO$_3$ with a ^{236}U concentration of c. 15 ng g^{-1}, and ^{204}Pb concentration of c. 1 ng g^{-1}. Each droplet is typically 30-40 mg, and spike will dissolve c. 10 % of its own mass in sample, providing the sample is in excess. Water used is 18.2 MΩ.cm and HNO$_3$ is distilled.
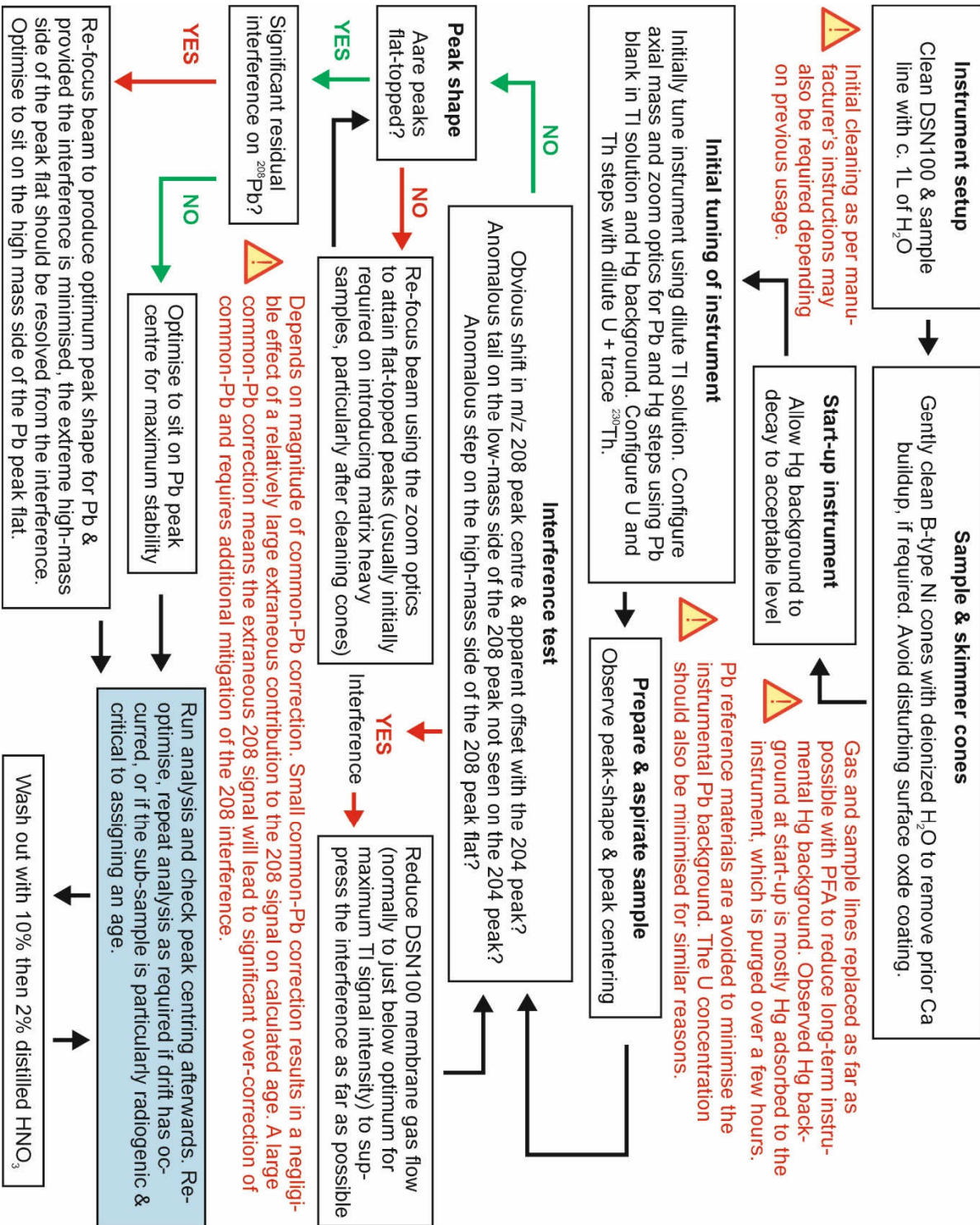
135   **Figure 2: flow chart U-Pb analytical protocol. Water used is 18.2 MΩ.cm unless otherwise stated.**

On the day of analysis, one-two drops (~30 µL drop volume; c. 15 pg µL^{-1} ^{236}U c. 1 pg µL^{-1} ^{204}Pb and 0.5 pg µL^{-1} ^{230}Th) of spike were added directly to the acid cleaned carbonate and gently agitated to mix as the spike dissolved the sample. Providing the sample is in excess of the HNO$_3$ in the spike, the spike dissolves c. 10% of its own mass of sample (i.e. c. 3-8

140   mg of sample is typically dissolved for the analysis), approximately fixing the sample to spike ratio. Although not critical to the age calculation, this does allow the absolute sample U concentration to be estimated without weighing, minimising sample handling. Once visible reaction with the spike was complete, the solution was diluted to around 15 ml with 18.2 MΩ.cm water, thoroughly shaken to homogenise and then immediately analysed, with no preconcentration of U and Pb. Dilution to c. 15 ml provides sufficient solution to check instrument set-up (see below) prior to analysis, allows replicate

145   analyses if needed, and mitigates matrix loading on the instrument.

Interferences are observed on Pb and must be monitored for (Fig 2). ^{204}Hg is an isobaric interference on ^{204}Pb that tends to be present as a persistent instrumental background on ICP-MS instruments. In our case, the long-term instrumental Hg background was substantially reduced by replacing gas and sample lines in the instrument and desolvator with acid cleaned

150   PFA tubing. Prior to an analytical session the instrument was run for several hours to volatilise Hg adsorbed to the instrument interface. A molecular interference has also been observed on Pb when samples are introduced, particularly on ^{208}Pb. The interference overlaps the Pb peak, but its centre is c. 0.15 AMU lighter than Pb such that the superposition of the interference peak is generally obvious, and it can be largely suppressed with appropriate tuning. Based on the mass offset, the interference is a molecular of a mid-mass element. Sr$_2$O$_2^+$ is suspected based on the group 2 element-rich sample matrix

155   and the relative magnitude at masses 208, 207, 206 etc. No evidence of interferences on U has been observed.

Table 1. Collector configuration for U-Pb analysis.

step	Axial							low mass	Integration time
	DVM6	DVM7	DVM8	IC0	DVM9	IC1	DVM10	IC2	
0				208		206		204	10s
1				207					10s
2				206		204		202	10s
3				204		202			10s
4		238		236	235				10s
5	238		236	235					10s
6				232		230			10s

DVM' collectors are Faraday collectors, 'IC' collectors are electron multiplier ion counters. Step 6 is option and can be omitted if the ^{232}Th is already known to be negligible in the sample (e.g. from a prior attempt at U-Th dating).

Analyses were carried out in a six-step routine with the magnet switched successively between steps (Table 1) for 10 or 15

160   repetitions. In steps 0-3 ^{208}Pb, ^{207}Pb, ^{206}Pb, ^{204}Pb+^{204}Hg and ^{202}Hg were measured on three ion-counters (ICx collectors in Table 1) separated by Faraday collectors (DVMx collectors in Table 1). The relative gains of the three ion counters were

determined based on the successive measurement of the mass-204 beam on each ion counter during the analysis. ^{202}Hg was monitored to correct for the ^{204}Hg interference. In steps 4-5 ^{238}U was measured on a Faraday collector, with ^{235}U and ^{236}U measured alternately on both Faraday and ion counter; the intention being that this gives the option of using the

165   Faraday/Faraday ^{238}U/^{235}U ratio or the Faraday/ion counter ^{238}U/^{235}U ratio (using the ^{236}U to calibrate the ion counter gain as needed) depending on ^{235}U signal intensity. An optional step with ^{232}Th in IC0 and ^{230}Th in IC1 (Table 1) can be added where estimation of sample ^{232}Th/U ratio is required (as a check ^{232}Th is negligible), if this is not already known (e.g. from a prior attempt at U-Th dating). Mass fractionation was estimated using the measured ^{238}U/^{235}U ratio of the samples and an assumed natural value of 137.75 (typical speleothem value from Hiess et al., 2012). Based on previous testing of the U-Pb

170   mass fractionation behaviour of this instrument (Mason and Henderson, 2010), the mass fractionation for Pb was assumed to be 2 ‰/AMU higher than for U. Samples were washed out with 10 % and 2 % distilled HNO$_3$ while the next sample was spiked. Analysis time was around 15 minutes.

Prior to first analysis (Fig. 2), the desolvator and sample lines were cleaned with 10 % HNO$_3$, 2 % HNO$_3$ and 18.2 MΩ.cm

175   water. A dedicated set of Ni cones reserved for very low level Pb work were used. These were gently cleaned by rinsing with DI water prior to use to remove excessive Ca build-up from the skimmer orifice, however, as far as possible, the surface coating on the cones was not disturbed. The instrument was then initially tuned and optimised with c.100 ppt Tl solution and 5 ppb CRM145 U solution. Pb was avoided to prevent re-contamination of the instrument and, sufficient Pb-blank is present in the Tl solution to see the Pb peaks on the ion counters. Instrumental Pb background could then be further reduced by

180   temporarily lowering the auxiliary gas flow (to c. 0.5 L min^{-1}) with RF power at 1300 Watts, allowing the plasma to run hot to 'evaporate' residual Pb from the instrument interface and, then, using relatively cool running conditions (auxiliary gas flow of 1.15 L min^{-1} and 1200-1250 Watts RF power). In some instances, this reduced the Pb background by a factor of >10×, without major loss of sensitivity. Peak shape and optimisation was then re-checked on actual samples – focusing settings for the zoom optics often changed substantially from the nominally clean Tl solution to the matrix-heavy samples,

185   especially following cleaning of the cones. Gas flows were also re-optimised to suppress the interference on ^{208}Pb. This was usually achieved by setting the desolvator gas flows such that the 'Hot Gas' flow was zero and, the membrane gas flow was slightly on the low side of the optimum for maximum signal intensity. Optimisation was then checked again after an initial couple of sacrificial analyses and then regularly during the course of the analytical session and, particularly when critical highly radiogenic samples with small ^{208}Pb beams were encountered. The DSN100 was re-cleaned with 18.2 MΩ.cm water

190   as required to remove U and Pb background or when sensitivity dropped due to Ca-loading of the membrane.

Where ^{235}U-^{207}Pb dating was the focus, the method was modified slightly to further mitigate the interference on ^{208}Pb. Although ^{208}Pb is not directly used in the age calculation, it is the basis for the common Pb correction, which ^{207}Pb is far more sensitive to than the ^{206}Pb, owing to the much lower production rate of radiogenic ^{207}Pb. Instead of optimising to be

centred on the Pb peaks, measurements were made on the extreme high-mass side of the peak flat. Provided the ion beam is
well-focused to give optimal peak shapes and the gas flows set to minimise the interference, the high-mass side of the peak
flat appears relatively 'clean'. The trade-off is that there is little margin for any drift in the magnet or degradation in the peak
geometry before the measurement is no longer on the peak flat, so more frequent evaluation of the optimisation is required.
However, because of the volume of sample solution prepared and the relatively short analysis time, having to reanalyse if
drift has occurred is not problematic.

3.3 Choice of tracer solution

We use a mixed ^{236}U-^{230}Th-^{204}Pb tracer for isotope dilution. Using the non-radiogenic ^{204}Pb as tracer allows the measurement
of the radiogenic ^{206}Pb and ^{207}Pb and, it is the least abundant of the four stable Pb isotopes in the samples. ^{204}Pb is also more
easily obtainable than artificial ^{205}Pb and ^{202}Pb. The instrumental Hg background also makes the small unspiked ^{204}Pb signal
unsuitable as a monitor for common Pb without preconcentration, so spiking with ^{204}Pb does not sacrifice any sample
information that would otherwise have been obtainable. Moreover, for ^{238}U-^{234}U-^{206}Pb chronology, using a tracer with ^{204}Pb
paired with artificial ^{236}U means that the critical ^{238}U/^{206}Pb ratio is determined from the ^{238}U/^{236}U and ^{206}Pb/^{204}Pb ratios, so it
is relatively insensitive to instrumental mass fractionation due to the mass difference for the natural/spike isotope being the
same for both U and Pb. For ^{238}U-^{234}U-^{206}Pb chronology on the instrument used, ^{204}Pb is also more favourable than ^{205}Pb
because it can be collected simultaneously on the ion-counters with ^{206}Pb, whereas ^{205}Pb cannot (Table 1). The disadvantage
of using ^{204}Pb is that sample ^{204}Pb must be corrected for, but this correction can be mitigated by adding sufficient spike ^{204}Pb
that the sample contribution is minor.

^{230}Th is included in the tracer to provide the option to measure ^{232}Th as a check that ^{208}Pb is unradiogenic. ^{230}Th is preferable
to artificial ^{229}Th because of the 2 AMU spacing of the ion counters on the instrument (Table 1). Again sample ^{230}Th needs
to be accounted for, but for samples in the U-Pb age range, sample ^{230}Th is likely to be close to equilibrium with ^{234}U.
Moreover, the ^{232}Th only needs to be measured semi-quantitatively as a check of the applicability of the method, and is not
used in the age calculation.

3.4 ^{234}U/^{238}U measurements for ^{238}U-^{234}U-^{206}Pb chronology

For ^{238}U-^{234}U-^{206}Pb chronology, aliquots of sample (usually including the residue from the U-Pb analysis) up to about 0.2 g
were dissolved and purified to obtain U cuts for measurement of the ^{234}U/^{238}U ratio. Dissolution was by the addition of 0.2
ml of 10 M HCl to the residual solution + residual carbonate. After obvious reaction had ceased, the solution was transferred
to clean 22 ml or 27 ml PFA vials and evaporated to dryness. The sample was then converted to chloride form by adding 1
ml 10 M HCl and again evaporating to dryness. Samples were then dissolved in 1 ml of 10 M HCl for loading onto columns
for separation of U. Purification used 2 ml Bio-Rad polyprep columns and an AG1X8 anion exchange resin bed of 2 ml.

Resin was batched pre-cleaned by suspending it in either 18.2 MΩ.cm H$_2$O or dilute HCl, allowing it to settle and decanting any residual suspended fines 8-10 times. Resin was then loaded into the column and cleaned sequentially with ~10 ml (column reservoir filled) 18.2 MΩ.cm H$_2$O, 10 M HCl and 18.2 MΩ.cm H$_2$O. The resin was then conditioned with two 4 ml aliquots of 10 M HCl, and the sample loaded and matrix Ca eluted with 2 x 5 ml aliquots of 10 M HCl. Sample U was eluted

230   with 2 x 5 ml aliquots of 18.2 MΩ.cm water and collected in the origin PFA vial (which was rinsed first with 18.2 MΩ.cm H$_2$O to remove the bulk of any residual sample Ca residue). The purified U was measured on the same instrument, with the ^{234}U and ^{238}U respectively measured on ion counter and Faraday collectors. Standard bracketing with CRM145 (CRM112a) was used to correct both for mass fractionation and ion counter gain.

235   Purification of the U is required because the ^{234}U/^{238}U ratio must be measured to a higher precision than the ^{238}U/^{206}Pb ratio. This requires preconcentration of the U to obtain a sufficiently large ^{234}U signal to ideally obtain better than 1 ‰ precision. Uranium, however, unlike Pb, is not blank sensitive, so the ion exchange procedure is relatively straightforward. Moreover, if the ^{234}U/^{238}U measurements are made after the U/Pb measurements, only those samples for which a ^{234}U/^{238}U measurement will be beneficial need be processed.

240   **3.5 Non-radiogenic Pb correction and Age calculation**

In order to obtain an accurate age, it is necessary to account for any non-radiogenic Pb (blank and sample common Pb) in an analysis. The main method used here is to employ an isochron-type approach in ^{208}Pb/^{206}Pb-^{238}U/^{206}Pb and ^{208}Pb/^{207}Pb-^{235}U/^{207}Pb isotope space, respectively for the ^{238}U-(^{234}U)-^{206}Pb and ^{235}U-^{207}Pb systems. ^{208}Pb is used as a proxy for the non-radiogenic ^{206}Pb (and ^{207}Pb), such that regression line intercepts with the axes yield the common ^{208}Pb/^{206}Pb (or ^{208}Pb/^{207}Pb)

245   and ^{238}U/radiogenic^{206}Pb (or ^{235}U/radiogenic^{207}Pb) ratios (see sections 5 and 6 for example plots). Once the common Pb composition of a sample suite is characterised, model ages for individual U-Pb analyses are calculated. Because the common Pb intercept of a regressions line can be fairly insensitive to variation in the radiogenic end-member if the regression includes unradiogenic analyses, only an approximation of an isochron may be needed to obtain the common Pb composition. Thus, for relatively large related sample sets, rather than devoting resources to a blanket isochron approach at the outset,

250   analyses are first made across the range of sample components to be dated (e.g. different layers from multiple speleothems from the same cave), then where possible, subsets of the data approximating to mixing lines are identified, from which the common Pb composition can be estimated. If further constraint of the U-Pb system is required, additional analyses (and isochrons) can then be targeted at specific samples or parts of samples as needed. Provided redundant subsamples have been cleaned, this targeting can be done to a substantial extent within an analytical session, avoiding prior reconnaissance of the

255   U-Pb system. Optionally, isochron ages can also be calculated from ^{238}U/radiogenic^{206}Pb (or ^{235}U/radiogenic^{207}Pb) intercept value where desired. Regressions use the method of York (1969).

Alternatively, Tera-Wasserburg space is used in which the age is determined without explicit common Pb correction, based on the intersection of an isochron with concordia (e.g. Roberts et al., 2017). This approach, however, is not favoured by us as it does not allow separate evaluation of the ^{238}U-(^{234}U)-^{206}Pb and ^{235}U-^{207}Pb systems but, is utilised here where necessitated to compare independently obtained data.

For relatively young samples in which ^{234}U/^{238}U disequilibrium can still be quantified, model ^{238}U-^{234}U-^{206}Pb ages are calculated from each corresponding pair of U-Pb and ^{234}U/^{238}U analyses, using the estimated common ^{208}Pb/^{206}Pb ratio for the sample set to correct for the total non-radiogenic ^{206}Pb, based on the measured ^{208}Pb/^{206}Pb ratio. In this instance, the initial ^{234}U/^{238}U ratio is calculated from the measured ^{234}U/^{238}U ratio as part of the age calculation in a way analogous to U-Th dating. For older material, model ^{238}U-^{206}Pb ages are calculated using an assumed initial ^{234}U/^{238}U ratio. Model ^{235}U-^{207}Pb ages are calculated in an equivalent way correcting for the total non-radiogenic ^{207}Pb in the analysis based on the sample ^{208}Pb/^{207}Pb ratio and the estimated common ^{208}Pb/^{207}Pb ratio. Where ^{235}U-^{207}Pb ages are calculated but no corresponding ^{238}U-^{234}U-^{206}Pb age can be determined, the ^{238}U→^{206}Pb system is solved for the initial ^{234}U/^{238}U ratio using the calculated ^{207}Pb/^{235}U age.

Model ages are calculated using an in-house implementation of the general decay equations given by Faure (1986), in which the decay chains are simplified to ^{238}U → ^{234}U → ^{230}Th → ^{226}Ra → ^{206}Pb and ^{235}U→ ^{231}Pa → ^{207}Pb. Initial ^{230}Th and ^{231}Pa were assumed to have been absent and initial ^{226}Ra was assumed to have been at equilibrium. Decay constants used are: ^{238}U: 1.55125×10^{-10}, ^{234}U: 2.82203×10^{-6}, ^{230}Th: 9.17055×10^{-6}, ^{226}Ra: 4.33488×10^{-4}, ^{235}U: 9.8485×10^{-10}, ^{231}Pa: 2.11583×10^{-5}, ^{232}Th: 4.9475×10^{-11} (Cheng et al., 1998, 2013; Steiger and Jäger, 1977) Age uncertainties were determined using a Monte Carlo approach to propagate analytical uncertainty and uncertainties arising from initial ratios such as the common Pb composition and initial U isotopic composition. A natural ^{208}Pb/^{204}Pb ratio of 37.1±10 (95% confidence level) was assumed when accounting for sample ^{204}Pb in the isotope dilution calculation; the large uncertainty is to cover reasonably foreseeable terrestrial isotopic variations. For most analyses, >99% of the total ^{204}Pb originated from the tracer, so the correction is small. Blank Pb is not separately corrected for and is dealt with as part of the total non-radiogenic Pb correction, however, given a number of analyses have yielded >99% radiogenic ^{206}Pb, the Pb blank can be considered a generally minor source of non-radiogenic Pb.

4 Protocol validation methodology and sampling

In the absence of suitable well-characterised carbonate reference materials during the period of method development, the validation of the new procedure required means other than the direct analysis of reference materials. As an alternative, we set four independent validation tests for the new method:

290   1) The new method must be able to produce data/ages consistent with measurements by a conventional isotope dilution approach with purification of U and Pb – i.e. not removing the matrix must have no appreciable impact on the resulting data/ages.

         2) The method must be able to generate U-Pb ages that vary systematically with stratigraphic order in samples where the successive growth intervals are resolvable.

295   3) In samples where the common Pb correction permits, the method must be able to generate concordant ^{238}U-^{234}U-^{206}Pb and ^{235}U-^{207}Pb ages.

         4) The method should replicate data obtained independently in a different laboratory.

These four tests have been performed on three samples: ASH-15, SLL10-6 and JOHO-1. A fourth sample, SB_pk142 is also
300 analysed as a case study for the application of the ^{235}U-^{207}Pb chronometer.

ASH-15 is a calcite flowstone comprising an upper relatively thin brownish layer overlying a more massive yellowish layer (Fig. 3) and originates from Ashalim cave, Negev Desert, Israel. The massive yellow layer has previously been independently analysed at the University of Melbourne (Vaks et al., 2013a) and the University of Oxford (Mason et al., 2013) and has an age of c. 3 Ma and a U concentration of c. 1.5 ppm; ^{232}Th is negligible (Mason et al., 2013). The latter data
305 set, obtained with purification of the U and Pb from the matrix, is compared to new data obtained using the new protocol (i.e. without matrix removal) as a preliminary test of not removing the matrix.

SLL10-6 is a high-U (6 to 43 ppm) calcite stalagmite from Ledenaya Lenskaya cave, Siberia (Vaks et al., 2020). The sample comprises several distinct layers designated from A to G, in order of increasing stratigraphic age and, mostly separated by
310 visible hiatuses (Fig. 3). All seven stratigraphic layers have been analysed using the new protocol. Five subsamples each from the F and G layers have also been purified and analysed using the method of Mason et al. (2013). This provides control data, such that the reproducibility of the F and G ages, with and without matrix separation, can be tested. The multilayer nature of the sample is additionally used to test the ability of the new method to produce ages in stratigraphic order, while the high-U nature of the sample makes it suitable for testing concordance of ^{238}U-^{234}U-^{206}Pb ages and ^{235}U-^{207}Pb ages.
315 Previous ^{232}Th/^{238}U measurements from this sample and, other samples from the same cave (Vaks et al., 2013b) give a maximum ^{232}Th/^{238}U ratio of 1.6×10^{-3} and indicates the radiogenic ^{208}Pb contribution is insignificant.

JOHO-1 (Fig. 3) is a fault vein calcite from the Middle East with a relatively low bulk U concentration of 0.3-0.5 ppm. The fault vein has been analysed independently at the University of Oxford using the new protocol described and, at the NERC
320 Isotope Geoscience Laboratory (NIGL), Keyworth, UK by laser ablation ICP-MS, following the methods of Roberts et al.

(2017). The laser ablation analyses targeted a domain that included material with a much higher U concentration (up to 25 ppm). The sample is used to test the new protocol via inter-laboratory comparison.
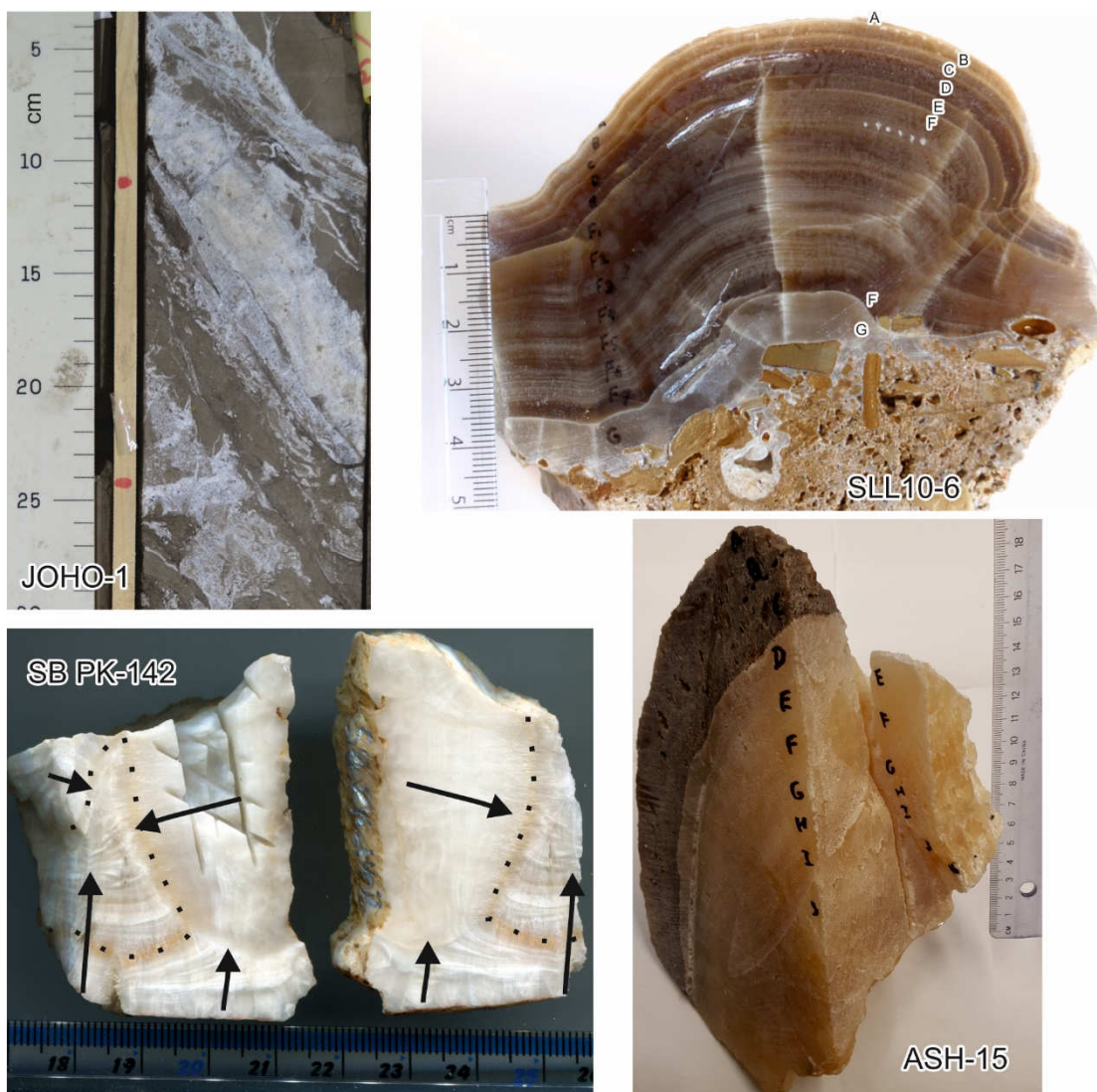
Figure 3: Samples: ASH-15 is a calcite flowstone from Ashalim Cave, Negev Desert. It comprises a lower yellow-orange unit c. 3 Ma old and a younger brown unit not analysed here. SLL10-6 is a calcite stalagmite from Ledyanaya Lenskaya Cave, Siberia. It comprises several layers designated A to G in order of increasing stratigraphic age, each apparently separated by a hiatus. SB_pk142 is an aragonitic speleothem comprising a flowstone that has merged in to two stalactites. The flowstone portion of the sample shows prominent lamination (sub-horizontal as viewed). The larger of the two stalactites forms the relatively featureless portion of the sample (with saw cuts on the left image). Remnants of a smaller stalactite form the extreme top left corner of the sample on the left image. The prominent iron oxide-stained layer (dashed line) separating stratigraphically older and younger parts of the sample should be noted. Arrows indicate growth direction. JOHO-1 is a calcite fault vein from the Middle East.

SB_pk142 (Fig. 3) is an aragonite speleothem from Botovskaya cave, Siberia. The sample consists of part of a stalactite that has merged in to flowstone, with the remains of a second smaller stalactite (now encased by the flowstone portion of the

335   sample) on one corner of the sample, and traces of reddish-brown clay on the stratigraphic base of the flowstone. The sample contains two stratigraphic domains separated by a prominent iron oxide-stained lamina, possibly representing a hiatus. Multiple subsamples from both stratigraphic domains have been analysed using the new method. A notable feature of speleothems from this cave is the large and variable ^{234}U excess, with known initial $^{234}U/^{238}U$ ratios ranging between 3.4 and 8.1 times equilibrium (Vaks et al., 2013b, 2020). This sample is used as an example application of the ^{235}U-^{207}Pb

340   chronometer to a cave system where the ^{238}U-^{206}Pb chronometer is problematic. Aragonite samples from Botovskaya cave show consistently low $^{232}Th/^{238}U$ ratios (<2e-4, Vaks et al., 2013b)), such that he radiogenic ^{208}Pb contribution is insignificant.

Detailed representative sample petrography for samples from Ledenaya Lenskaya and Botovskaya caves, as well as details

345   of the caves themselves is given in Vaks et al. (2013b, 2020).
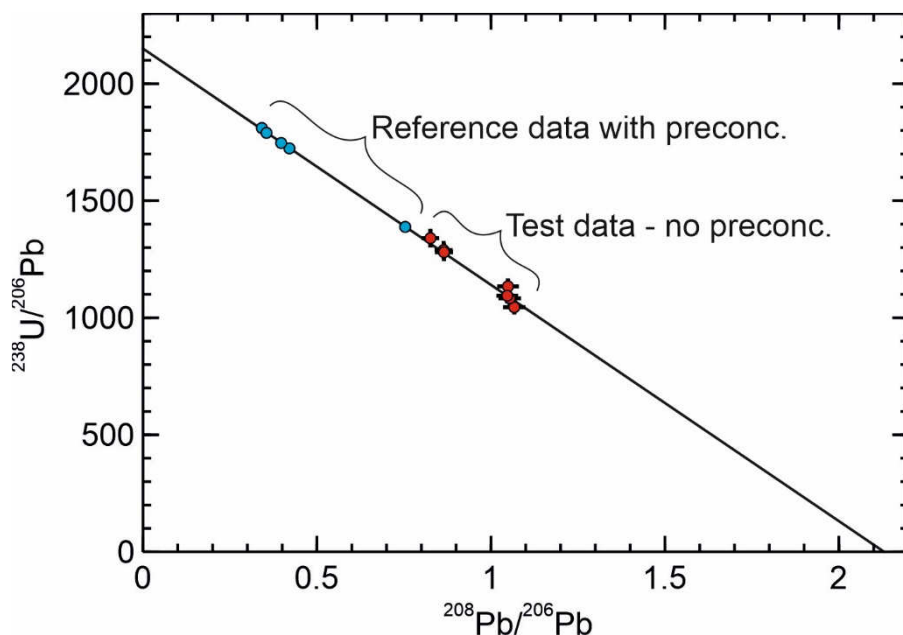
Figure 4: Preliminary data showing comparison of data obtained with the new method with no preconcentration with published data obtained with preconcentration (Mason et al., 2013). The critical result is that the data produced using the new method are
350   **co-linear with the data obtained with preconcetration and define a common isochron. The intersection of the isochron with the $^{208}Pb/^{206}Pb$ axis gives the common $^{208}Pb/^{206}Pb$ ratio and the intersection with the $^{238}U/^{206}Pb$ axis gives the $^{238}U/radiogenic^{206}Pb$ ratio providing the ^{208}Pb is entirely unradiogenic.**

5 Protocol validation results

5.1 ASH-15

Results for ASH-15 are given in Table 2 and Fig. 4. These analyses were intended as a preliminary test that the new U-Pb measurement procedure without matrix separation produces data consistent with published data (Mason et al., 2013) obtained using the same spike but with purification of U and Pb from the matrix. The new analyses are slightly less radiogenic than the analyses of (Mason et al., 2013), however, they are not exact replicates of the same subsamples, so some variation in the proportion of common Pb can be expected. The critical feature is that the data with and without matrix separation are co-linear defining a common isochron (Fig. 4) and are therefore consistent.
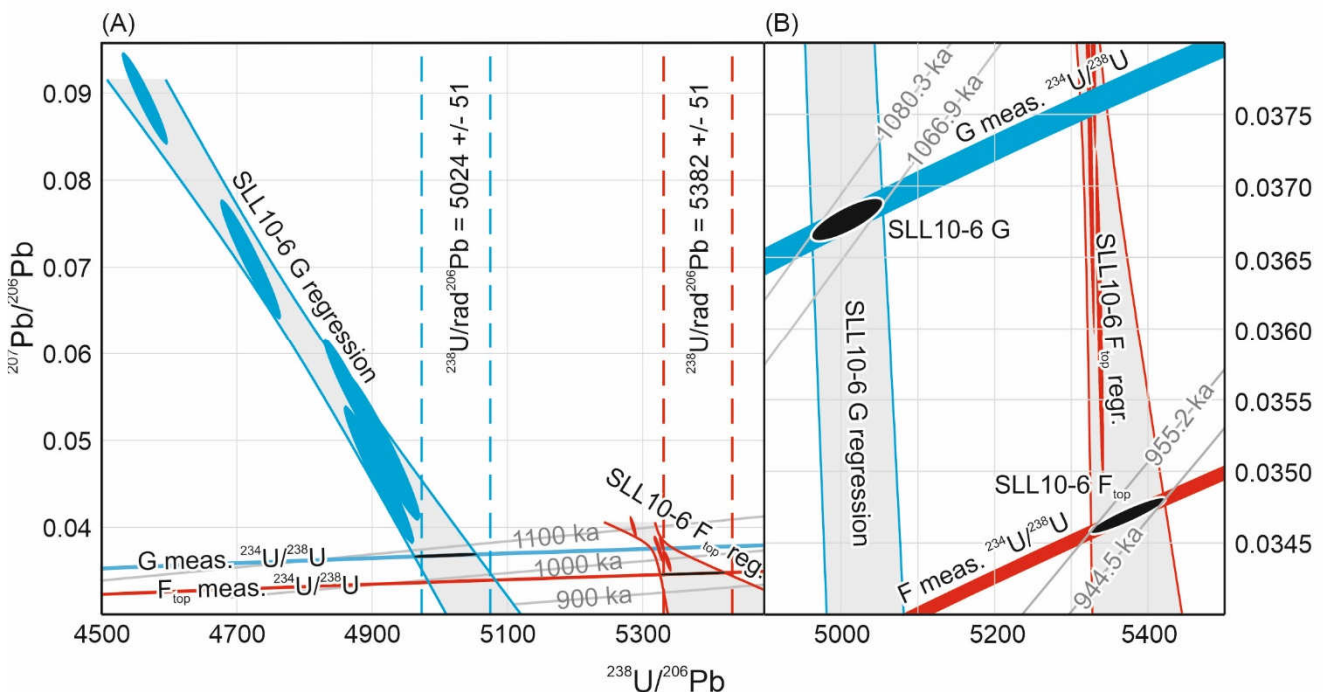
Figure 5: A) Modified Tera-Wasserburg diagram showing the control data for SLL10-6 G and F layers obtained with purification of the U and Pb from the matrix following the method of (Mason et al., 2013). Because the initial $^{234}U/^{238}U$ ratio is not known *a priori* a unique concordia curve appropriate to each sample layer cannot be defined. Instead two sets of tie-lines (the sub-horizontal curves) connecting concordia curves (not shown) with different initial $^{234}U/^{238}U$ ratios are plotted. The first set connect points of equal $^{234}U/^{238}U$ ratio for values corresponding to the mean measured $^{234}U/^{238}U$ ratio (+/- uncertainty) for the F and G layers. The second set of tie lines are age contours connecting points of equal age. The interpreted radiogenic $^{238}U/^{206}Pb$ and radiogenic $^{207}Pb/^{206}Pb$ ratios must simultaneously satisfy the tie-line corresponding to the measured $^{234}U/^{238}U$ ratio, and the mixing trend with common Pb defined by the regression fits (grey shaded bands) to the measured U-Pb data – i.e. the intersections shown with the black ellipses. The age is then defined by where the intersection falls in relation to the age contours. The vertical dashed lines indicate the radiogenic $^{238}U/^{206}Pb$ ratios interpreted from regression intercepts in $^{208}Pb/^{206}Pb$-$^{238}U/^{206}Pb$ isotope space (not shown but equivalent to Fig 8a) as a cross-check, and are consistent with the aforementioned intersections. B) Enlargement of the intersections between the regression fits to the measured data and the equal $^{234}U/^{238}U$ tie-lines for the sample measured $^{234}U/^{238}U$ ratios. Age contours correspond to the maximum and minimum ^{238}U-^{234}U-^{206}Pb age defined by the intersections for each sample. Calculations assume $^{238}U/^{235}U$=137.75, no initial ^{231}Pa or ^{230}Th and equilibrium initial ^{226}Ra.
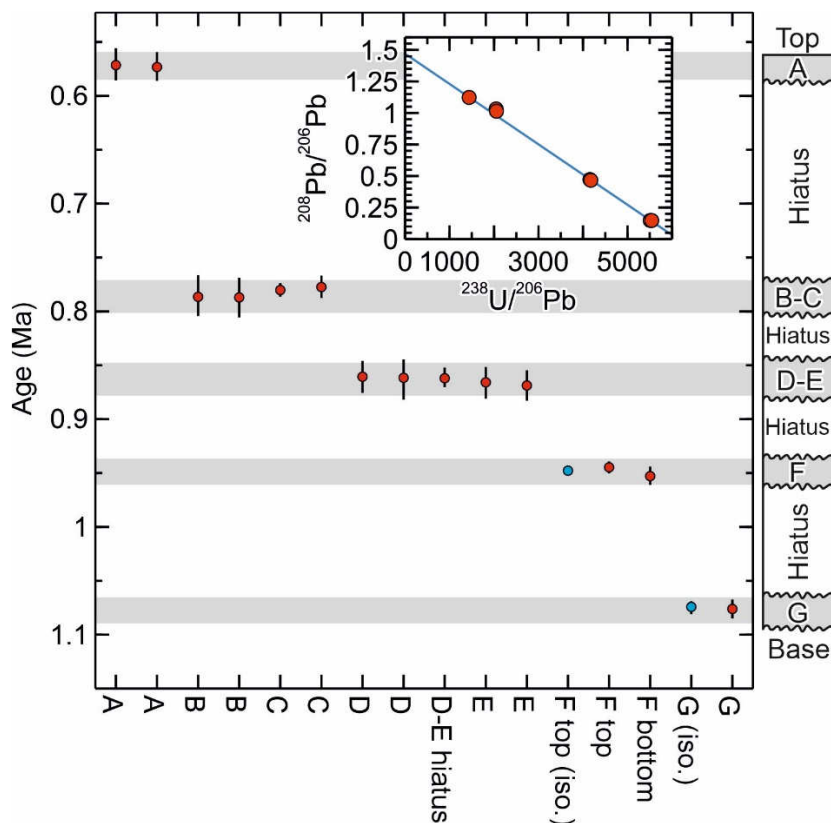
Figure 6: Summary data for SLL10-6 showing the replication of the ages from the layers F & G obtained using the method of Mason *et al.* (2013) (ages with 'iso.' label) with the ages obtained using the new method, and the consistency of the ages produced with the new method with the stratigraphic order of the samples. The inset shows isotopic data from the layers B & C which includes some of the least radiogenic analyses obtained from this cave, and were used to help to constrain the common $^{208}Pb/^{206}Pb$ to c. 1.5 ($^{208}Pb/^{206}Pb$ axis intercept).

5.2 SLL10-6

Control data for the F and G layers obtained with purification of U and Pb from the matrix following the method of Mason et al. (2013) are given in Table 2 and Fig. 5. Data and ages obtained using the new analytical methodology for all layers of SLL10-6 are also given in Table 2, and Fig. 6.

The control data yield ^{238}U-^{234}U-^{206}Pb isochron ages of 1073.6 +/-6.7 ka and 949.9 +/- 5.4 ka (95% conf.) respectively for the G layer and the upper part of the F layer. The corresponding ages for the G layer and the upper part of the F layer obtained using the new protocol are 1076.2 +8.5/-8.8 ka and 944.7 +5.6/-5.6 ka respectively. The ^{238}U-^{234}U-^{206}Pb ages therefore replicate with an uncertainty of better than 1 %, irrespective of whether the matrix is removed or not.

^{238}U-^{234}U-^{206}Pb ages for SLL10-6 obtained using the new protocol vary systematically from 1076.2 +8.5/-8.8 ka near the stratigraphic base of the sample to 571.4 +13.7/-14.4 ka near the stratigraphic top of the sample, with no age reversals.

395   Treating replicate and overlapping ages as single values, five distinct age values are observed. The likelihood of these ages falling in stratigraphic order as the consequence of a fluke result is, thus, 1 in 5!, or less than 1%.

^{235}U-^{207}Pb ages obtained for SLL10-6 using the new method are less precise than the ^{238}U-^{234}U-^{206}Pb ages owing mainly to the proportionally much larger common Pb correction on ^{207}Pb. Nevertheless, the most radiogenic analyses, layer G and F$_{top}$

400   yield reasonable ^{235}U-^{207}Pb ages of 1060 +46/-48 ka and 960 +47/-54 ka respectively, in agreement with the corresponding ^{238}U-^{234}U-^{206}Pb ages of 1076.2 +8.5/-8.8 ka and 944.7 +5.6/-5.6 ka. All other obtained ^{235}U-^{207}Pb ages are also concordant with their corresponding ^{238}U-^{234}U-^{206}Pb ages.
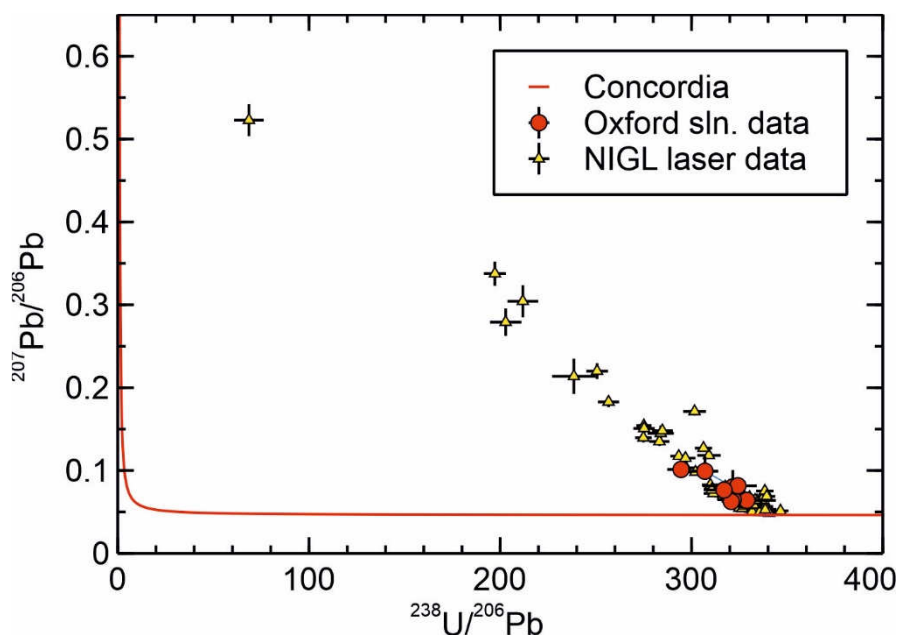
405   **Figure 7: Tera-Wasserburg diagram showing a comparison of data from sample JOHO-1 obtained at NIGL by LA ICP-MS with data obtained at Oxford using the new method. Data are presented in ^{238}U/^{206}Pb – ^{207}Pb/^{206}Pb isotope space for compatibility with the NIGL LA data and because no independent measurement of the ^{232}Th/^{238}U is presently available. Equilibrium concordia is shown for reference. The co-linearity of the Oxford and NIGL data indicate the consistency of the two data sets. The intersection of the array of data with concordia at ^{238}U/^{206}Pb c. 340 and ^{207}Pb/^{206}Pb c. 0.05 gives the radiogenic end member without the use of a**
410   **purely unradiogenic Pb isotope, but at the expense of obtaining independent ^{235}U/^{207}Pb ages. The intersection with concordia corresponds to an age of c. 19.25 Ma, assuming equilibrium initial ^{234}U.**

5.3 JOHO-1

Results for JOHO-1 are given in Table 2 and Fig. 7. The results are intended as an inter-laboratory comparison of isotopic

415   measurements made using the new protocol at the University of Oxford, with those obtained independently at NIGL by laser ablation. Results are given in terms of $^{238}U/^{206}Pb$-$^{207}Pb/^{206}Pb$ ratios for compatibility with the NIGL laser ablation measurements. The NIGL data define a mixing trend from highly radiogenic compositions (with a $^{238}U/^{206}Pb$ ratio of c. 340 and a $^{207}Pb/^{206}Pb$ ratio of c. 0.05) falling just above Concordia, towards a common Pb $^{207}Pb/^{206}Pb$ ratio of c.0.65, but with the majority of the analyses clustering towards the radiogenic end of the trend. The Oxford data fall towards the radiogenic end

420   of the same trend and are thus consistent with the NIGL analyses and yield a comparable age if common assumptions are used. Thus, for example, regression of each data set through a common $^{207}Pb/^{206}Pb$ ratio of 0.65+/-0.1 yields concordia intercepts at 19.34 +/- 0.30 Ma and 19.19 +/- 0.15 Ma respectively for the Oxford solution data and NIGL laser ablation data respectively (concordia assumes no initial ^{230}Th or ^{231}Pa and equilibrium initial ^{234}U and ^{226}Ra). Less spread towards unradiogenic compositions is seen in the Oxford data, but this is unsurprising given that fewer analyses were made.

6 SB_pk142 results

425

Results for SB_pk142 from Botovskaya cave are shown in Fig. 8 and Table 2. On a $^{208}Pb/^{206}Pb$-$^{238}U/^{206}Pb$ plot data from SB_pk142 fall on two distinct trends corresponding to the stratigraphically older and younger sections of the sample. The stratigraphically older part of the sample has a consistently lower $^{238}U/^{206}Pb$ ratio for a given $^{208}Pb/^{206}Pb$ ratio than the stratigraphically younger section. The intercept $^{238}U/^{206}Pb$ values of the two trends at c. 685 and c. 910, respectively for the

430   older and younger sections of the sample correspond to apparent ^{238}U-^{206}Pb ages of c. 9.5 Ma and 7.5 Ma, assuming equilibrium initial ^{234}U and no initial ^{230}Th. The assumption that initial ^{234}U was in equilibrium is likely incorrect (see below) but demonstrates the point that there is an appreciable apparent age difference between the older and younger sections of the sample, which appears consistent with the apparent hiatus, and the age order superficially agrees with the stratigraphy of the sample. The common $^{208}Pb/^{206}Pb$ ratio suggested by the upper and lower sections of the sample are not appreciably different.

435

On a $^{208}Pb/^{207}Pb$-$^{235}U/^{207}Pb$ plot data from SB_pk142 shows a rather different pattern and the data from both the stratigraphically older and younger portions of the sample define a single trend with an intercept of c. 171.2. This corresponds to a $^{235}U/^{207}Pb$ age of c. 6 Ma, and suggests the stratigraphically older and younger portions of the sample are not, in fact, appreciably different in age, and that the sample is rather younger than the ^{238}U-^{206}Pb system suggests.
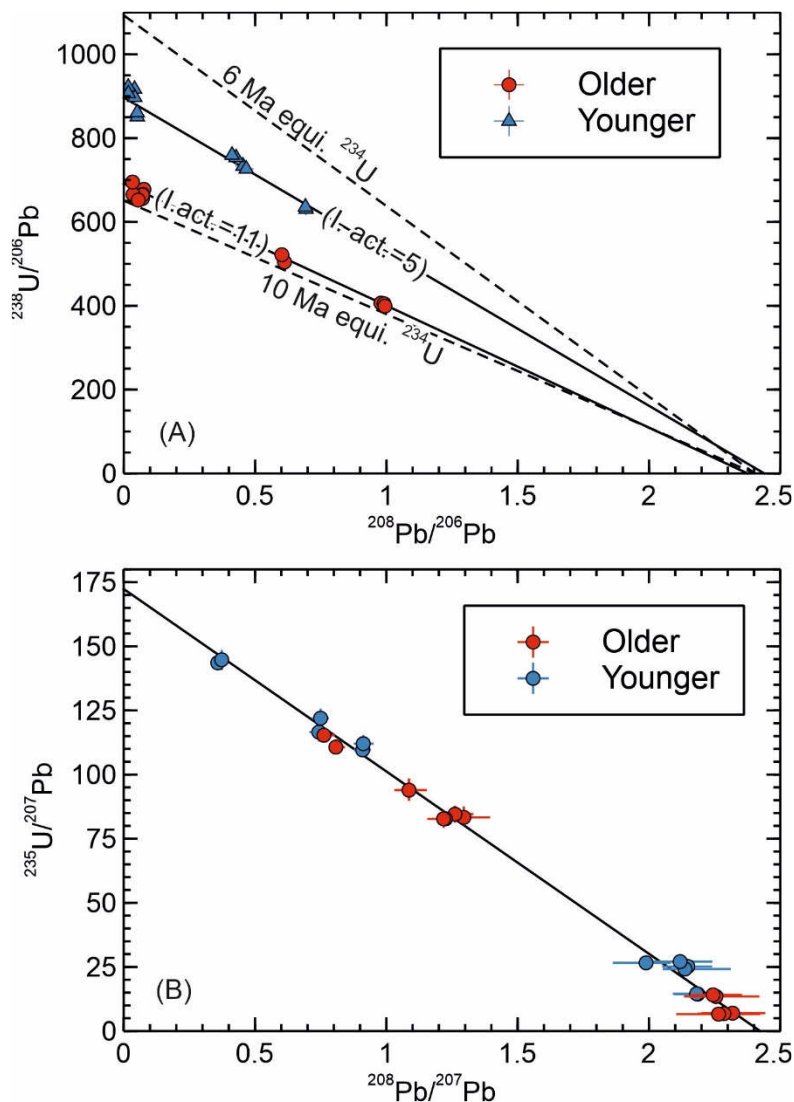
Figure 8: Isochron plots for sample SB_pk142. The 'older' and 'younger' sections are respectively stratigraphically older and younger than an iron oxide-stained lamina possibly marking a hiatus. Based on the maximum ^{232}Th/^{238}U observed for aragonite samples in this cave (Vaks et al., 2013a), ingrown ^{208}Pb is estimated to make no more than a c. 3 ‰ contribution to the ^{208}Pb/^{206}Pb and ^{208}Pb/^{207}Pb ratios for the most radiogenic analyses, becoming inconsequential for the least radiogenic analyses. This contribution is negligible for the common Pb correction and has a maximum effect on the (^{235}U-^{207}Pb) age of ~0.5 ‰. In both plots the isochron intersection with the x-axis corresponds to the common Pb composition, while, in the effective absence of ingrown ^{208}Pb, the intersection with the y-axis corresponds to the ^{23x}U/radiogenic ^{20y}Pb ratio. A) ^{208}Pb/^{206}Pb-^{238}U/^{206}Pb plot showing the two portions of the sample falling on clearly distinct trends corresponding to apparent ^{238}U -^{206}Pb ages of c. 7.2 Ma and c. 9.5 Ma. The dashed lines are reference isochrons for 6 Ma and 10 Ma assuming equilibrium initial ^{234}U. The figures in brackets are the initial ^{234}U/^{238}U activity ratios associated with each portion of the sample, estimated by solving the ^{238}U-^{206}Pb decay equation using the ^{235}U-^{207}Pb age. B) ^{208}Pb/^{207}Pb-^{235}U/^{207}Pb plot showing the two sections of the sample falling on a common trend, suggesting they actually have a similar age of c. 6 Ma. The 6 Ma reference isochron on Fig. 8A is considered to represent the true age of the sample based on the ^{235}U-^{207}Pb data. The plotting of the data on two separate and apparently older isochrons in Fig. 8A is attributable to the distinct and high initial ^{234}U/^{238}U ratios in the two parts of the sample, which resulted in two populations of data with different radiogenic ^{206}Pb excesses relative to the 6 Ma reference isochron.

The data show basically coherent mixing lines between a radiogenic end-member and common Pb, thus, the discrepancy between the ^{238}U-^{206}Pb system and ^{235}U-^{207}Pb system cannot be easily attributed to open system behaviour. Moreover, such an explanation would require U or Pb isotopes from the two systems to have behaved differently. Extreme ^{234}U disequilibrium is, however, known to occur in samples from Botovskaya cave, with initial ^{234}U/^{238}U ratios between 3.4 and

460   8.1 times equilibrium reported for samples from the last 0.5 Ma based on U/Th dating (Vaks et al., 2013b, 2020). Excess ^{206}Pb from the decay of excess initial ^{234}U will make the ^{238}U/radiogenic^{206}Pb ratio appear low (old) compared to the corresponding ^{235}U/radiogenic^{207}Pb ratio, with the discrepancy depending on the initial ^{234}U/^{238}U ratio; in other words it allows time-independent variation of the ^{238}U/radiogenic^{206}Pb ratio not seen in the ^{235}U/^{207}Pb ratio. This could account for older apparent ^{238}U-^{206}Pb ages and the difference between the ^{208}Pb/^{206}Pb-^{238}U/^{206}Pb and ^{208}Pb/^{207}Pb-^{235}U/^{207}Pb plots.

465   Excluding subsamples 15-17, which are unradiogenic, the upper section of the sample gives a mean ^{235}U-^{207}Pb model age of 5.9 Ma with typical uncertainties on individual ^{235}U/^{207}Pb model ages of +/- 0.2 to 0.3 Ma, and suggests an initial ^{234}U/^{238}U ratio varying between 3.8 and 5.8 times equilibrium (Table 2). This initial ^{234}U/^{238}U is typical of that already documented from Botovskaya cave. The lower section of the sample is generally slightly less radiogenic, but where subsamples yield ^{235}U/^{207}Pb ages they are indistinguishable from the upper section of the sample. Calculated initial ^{234}U/^{238}U ratios for the

470   lower part of the sample are higher than those previously reported but not particularly unexpected for this cave, at between 10 and 11.6 times equilibrium. It is uncertain why the initial ^{234}U/^{238}U changed between the two sections of the sample, though the fact that a prominent iron oxide-stained lamina separates the two portions of the sample seems to indicate a change in growth conditions occurred.

475   **Table 2. U-Pb data and ages**

Table 2a. Preliminary test data for ASH-15 obtained without preconcentration of U and Pb.

	^{238}U/^{206}Pb	+	-	^{208}Pb/^{206}Pb	+	-
ASH-15I_1	1045	31	31	1.067	0.032	0.032
ASH-15I_1 (replicate)	1083	32	32	1.054	0.032	0.032
ASH-15I_2	1289	39	39	0.864	0.026	0.026
ASH-15I_3	1280	38	38	0.865	0.026	0.026
ASH-15I_4	1340	40	40	0.826	0.025	0.025
ASH-15I_5	1134	34	34	1.049	0.031	0.031
ASH-15I_5 (replicate)	1094	33	33	1.047	0.031	0.031

Uncertainties are 95% confidence

Table 2b. Isochron reference data for SLL10-6 F and G obtained with preconcentration of U and Pb. Each analysis is a separate subsample.

ID	$^{238}U/$ ^{206}Pb	+	-	$^{207}Pb/$ ^{206}Pb	+	-	ρ ($^{238}U/$ ^{206}Pb- $^{207}Pb/$ ^{206}Pb)[a]	$^{208}Pb/$ ^{206}Pb	+	-	ρ ($^{238}U/$ ^{206}Pb- $^{208}Pb/$ ^{206}Pb)[a]
SLL10-F-top	5328	4	3	0.03813	0.00069	0.00074	-0.71	0.0095	0.0012	0.0012	-0.72
SLL10-F-top	5325	5	4	0.03724	0.00100	0.00109	-0.84	0.0072	0.0018	0.0019	-0.85
SLL10-F-top	5337	4	5	0.03606	0.00100	0.00095	-0.79	0.0051	0.0017	0.0016	-0.80
SLL10-F-top	5320	3	3	0.03838	0.00053	0.00059	-0.63	0.0107	0.0010	0.0010	-0.64
SLL10-F-top	5286	4	4	0.04010	0.00098	0.00100	-0.81	0.0150	0.0018	0.0016	-0.82
SLL10-6-G	4720	40	34	0.07089	0.00519	0.00613	-0.95	0.0884	0.0131	0.0150	-0.98
SLL10-6-G	4564	30	26	0.08938	0.00397	0.00475	-0.95	0.1347	0.0100	0.0113	-0.97
SLL10-6-G	4910	46	40	0.04604	0.00610	0.00695	-0.96	0.0245	0.0154	0.0168	-0.98
SLL10-6-G	4915	49	42	0.04927	0.00643	0.00737	-0.96	0.0328	0.0163	0.0181	-0.98
SLL10-6-G	4872	39	32	0.05525	0.00488	0.00579	-0.96	0.0484	0.0123	0.0141	-0.98

480   Table 2b continued.

ID	$^{235}U/$ ^{207}Pb	+	-	$^{208}Pb/$ ^{207}Pb	+	-	ρ ($^{235}U/$ ^{207}Pb-$^{208}Pb/$ ^{207}Pb)[a]	$^{234}U/$ ^{238}U	+	-
SLL10-F-top	1002	20	19	0.249	0.027	0.028	-0.93	5.9241E-05	7.0E-08	6.2E-08
SLL10-F-top	1026	32	28	0.194	0.042	0.046	-0.96	5.9223E-05	6.6E-08	6.7E-08
SLL10-F-top	1061	29	29	0.140	0.044	0.043	-0.96	5.9202E-05	6.6E-08	6.4E-08
SLL10-F-top	994	16	14	0.278	0.022	0.021	-0.91	5.9192E-05	5.9E-08	5.9E-08
SLL10-F-top	945	25	24	0.373	0.034	0.034	-0.94	5.9187E-05	6.0E-08	5.7E-08
Mean								5.9209E-05	2.8E-08	2.8E-08
SLL10-6-G	484	49	37	1.246	0.090	0.118	-0.93	5.7588E-05	6.5E-08	8.9E-08
SLL10-6-G	371	23	18	1.507	0.044	0.058	-0.88	5.7587E-05	6.0E-08	8.5E-08
SLL10-6-G	778	142	100	0.523	0.241	0.329	-0.97	5.7610E-05	5.7E-08	9.0E-08
SLL10-6-G	727	132	92	0.659	0.222	0.308	-0.97	5.7548E-05	6.2E-08	8.5E-08
SLL10-6-G	642	79	57	0.873	0.138	0.185	-0.96	5.7535E-05	6.2E-08	8.5E-08
Mean								5.7574E-05	3.9E-08	3.9E-08

Uncertainties are empirical 95% confidence Monte Carlo errors. The slight variations in the model values for different samples are random fluctuations arising from the Monte Carlo approach. Data are corrected for procedural balnk.
[a]Correlation coefficient for the uncertainties on the specified ratio pairs.

Table 2c. U-Pb data, ^{238}U-^{234}U-^{206}Pb ages and ^{235}U-^{207}Pb ages for SLL10-6 obtained without preconcentration of U and Pb.

ID	^{238}U/ ^{206}Pb	+	-	^{234}U/ ^{206}Pb	+	-	^{208}Pb/ ^{206}Pb	+	-	ρ (^{238}U/ ^{206}Pb- ^{208}Pb/ ^{206}Pb)[a]	ρ (^{234}U/ ^{206}Pb- ^{208}Pb/ ^{206}Pb)[a]
SLL10-6 A	5741	65	71	0.3839	0.0043	0.0049	0.5001	0.0044	0.0045	-0.21	-0.21
SLL10-6 A	5777	97	96	0.3863	0.0065	0.0064	0.4987	0.0096	0.0093	0.07	0.07
SLL10-6 B	2047	169	158	0.1279	0.0106	0.0099	1.0315	0.0557	0.0547	-0.05	-0.05
SLL10-6 B	2054	146	133	0.1284	0.0091	0.0083	1.0144	0.0439	0.0436	-0.04	-0.04
SLL10-6 B re-cleaned	4156	71	73	0.2596	0.0045	0.0046	0.4725	0.0139	0.0119	0.14	0.14
SLL10-6 B re-cleaned	4175	75	92	0.2608	0.0047	0.0057	0.4664	0.0132	0.0106	-0.11	-0.11
SLL10-6 B-C hiatus	1441	35	67	0.0901	0.0022	0.0042	1.1233	0.0100	0.0090	-0.40	-0.40
SLL10-6 C	5546	116	110	0.3480	0.0074	0.0069	0.1473	0.0052	0.0028	0.04	0.04
SLL10-6 C	5509	60	59	0.3457	0.0038	0.0037	0.1479	0.0027	0.0018	-0.05	-0.05
SLL10-6 D re-cleaned	4561	129	172	0.2788	0.0080	0.0106	0.2768	0.0074	0.0073	-0.13	-0.13
SLL10-6 D re-cleaned	4585	96	108	0.2803	0.0058	0.0066	0.2723	0.0088	0.0060	0.16	0.16
SLL10-6 D-E hiatus	4683	44	39	0.2870	0.0027	0.0024	0.2345	0.0096	0.0056	0.06	0.06
SLL10-6 E	4324	74	112	0.2639	0.0045	0.0068	0.3369	0.0067	0.0057	-0.30	-0.30
SLL10-6 E	4315	72	82	0.2633	0.0044	0.0051	0.3329	0.0048	0.0052	0.18	0.18
SLL10-6 F top	5165	45	44	0.3057	0.0026	0.0026	0.0712	0.0016	0.0015	0.21	0.20
SLL10-6 F bottom	4543	48	43	0.2699	0.0029	0.0026	0.2035	0.0028	0.0024	-0.16	-0.16
SLL10-6 G	4838	59	56	0.2782	0.0034	0.0032	0.0545	0.0019	0.0015	-0.01	-0.01

485   Table 2c continued.

ID	^{234}U/ ^{238}U	+	-	Model com. ^{208}Pb/ ^{206}Pb[b]	+	-	^{238}U- ^{234}U- ^{206}Pb age (Ma)	+	-
SLL10-6 A	6.6867E-05	1.3E-07	1.2E-07	1.471	0.100	0.102	0.5732	0.0130	0.0141
SLL10-6 A	6.6868E-05	1.3E-07	1.3E-07	1.470	0.098	0.096	0.5714	0.0137	0.0144
SLL10-6 B	6.2476E-05	5.8E-08	5.9E-08	1.470	0.100	0.096	0.7325	0.0907	0.1026
SLL10-6 B	6.2475E-05	5.7E-08	5.9E-08	1.472	0.098	0.101	0.7494	0.0791	0.0938
SLL10-6 B re-cleaned	6.2475E-05	6.0E-08	6.0E-08	1.470	0.099	0.099	0.7863	0.0177	0.0193
SLL10-6 B re-cleaned	6.2475E-05	6.0E-08	5.9E-08	1.471	0.100	0.101	0.7872	0.0186	0.0187
SLL10-6 B-C hiatus	6.2559E-05	5.3E-08	5.1E-08	1.471	0.100	0.100	0.7840	0.0927	0.1169
SLL10-6 C	6.2759E-05	5.7E-08	5.8E-08	1.471	0.100	0.099	0.7774	0.0099	0.0103
SLL10-6 C	6.2760E-05	5.9E-08	5.9E-08	1.470	0.097	0.103	0.7802	0.0062	0.0064
SLL10-6 D re-cleaned	6.1141E-05	5.8E-08	5.7E-08	1.470	0.099	0.100	0.8615	0.0199	0.0171
SLL10-6 D re-cleaned	6.1141E-05	5.6E-08	5.6E-08	1.472	0.101	0.101	0.8609	0.0149	0.0143
SLL10-6 D-E hiatus	6.1277E-05	5.1E-08	5.2E-08	1.471	0.098	0.098	0.8620	0.0081	0.0098
SLL10-6 E	6.1021E-05	5.7E-08	5.7E-08	1.470	0.102	0.097	0.8657	0.0153	0.0140
SLL10-6 E	6.1021E-05	5.7E-08	5.7E-08	1.471	0.102	0.100	0.8687	0.0146	0.0142
SLL10-6 F top	5.9194E-05	5.0E-08	4.9E-08	1.471	0.100	0.099	0.9447	0.0056	0.0056
SLL10-6 F bottom	5.9397E-05	5.0E-08	5.0E-08	1.470	0.101	0.100	0.9528	0.0081	0.0087
SLL10-6 G	5.7497E-05	4.8E-08	4.9E-08	1.471	0.099	0.102	1.0762	0.0085	0.0088

Table 2c continued.

ID	Initial ^{234}U/ ^{238}U	+	-	^{235}U/ ^{207}Pb	+	-	^{208}Pb/ ^{207}Pb	+	-	ρ (^{235}U/ ^{207}Pb- ^{208}Pb/ ^{207}Pb)[a]
SLL10-6 A	1.150E-04	2.2E-06	2.3E-06	186.7	2.9	2.9	2.240	0.059	0.044	0.72
SLL10-6 A	1.146E-04	2.4E-06	2.4E-06	183.4	4.6	4.6	2.180	0.079	0.079	0.74
SLL10-6 B	1.147E-04	1.7E-05	1.5E-05	32.5	3.8	4.0	2.255	0.363	0.315	0.76
SLL10-6 B	1.175E-04	1.5E-05	1.5E-05	34.6	4.2	3.4	2.355	0.340	0.306	0.82
SLL10-6 B re-cleaned	1.240E-04	3.5E-06	3.7E-06	143.3	4.0	3.9	2.244	0.121	0.091	0.79
SLL10-6 B re-cleaned	1.242E-04	3.7E-06	3.6E-06	140.8	4.7	6.4	2.167	0.075	0.099	0.58
SLL10-6 B-C hiatus	1.249E-04	2.0E-05	2.0E-05	22.2	0.7	0.7	2.390	0.073	0.057	0.27
SLL10-6 C	1.248E-04	2.0E-06	2.0E-06	453.7	12.3	12.5	1.661	0.061	0.059	0.55
SLL10-6 C	1.254E-04	1.3E-06	1.3E-06	439.8	14.2	17.2	1.626	0.082	0.068	0.91
SLL10-6 D re-cleaned	1.252E-04	4.1E-06	3.3E-06	239.1	9.4	10.2	2.000	0.101	0.103	0.57
SLL10-6 D re-cleaned	1.250E-04	3.0E-06	2.8E-06	242.8	7.1	10.6	1.988	0.080	0.103	0.72
SLL10-6 D-E hiatus	1.268E-04	1.7E-06	2.0E-06	283.8	4.3	3.7	1.957	0.094	0.057	0.29
SLL10-6 E	1.246E-04	3.1E-06	2.7E-06	191.4	5.1	5.5	2.055	0.093	0.085	0.74
SLL10-6 E	1.252E-04	2.9E-06	2.8E-06	195.3	5.6	5.5	2.076	0.080	0.068	0.83
SLL10-6 F top	1.157E-04	1.0E-06	9.7E-07	598.8	11.4	11.0	1.137	0.022	0.023	0.26
SLL10-6 F bottom	1.201E-04	1.5E-06	1.6E-06	288.5	5.0	5.5	1.780	0.039	0.035	0.56
SLL10-6 G	1.076E-04	1.3E-06	1.3E-06	614.3	8.8	9.1	0.953	0.034	0.028	0.33

490 Table 2c continued.

ID	Model com. ^{208}Pb/ ^{207}Pb[b]	+	-	Model ^{238}U/ ^{235}U	+	-	^{207}Pb- ^{235}U age (Ma)	+	-	^{207}Pb/ ^{206}Pb	+	-
SLL10-6 A	2.463	0.137	0.136	137.75	0.19	0.20				0.2233	0.0043	0.0046
SLL10-6 A	2.465	0.136	0.136	137.75	0.20	0.20	0.683	0.327	0.343	0.2288	0.0062	0.0063
SLL10-6 B	2.463	0.138	0.137	137.75	0.20	0.20				0.4592	0.0681	0.0609
SLL10-6 B	2.465	0.135	0.133	137.75	0.20	0.21				0.4325	0.0577	0.0536
SLL10-6 B re-cleaned	2.467	0.135	0.140	137.75	0.20	0.20				0.2105	0.0068	0.0067
SLL10-6 B re-cleaned	2.464	0.131	0.134	137.75	0.20	0.20	0.916	0.424	0.429	0.2153	0.0074	0.0060
SLL10-6 B-C hiatus	2.463	0.136	0.129	137.75	0.20	0.20				0.4700	0.0108	0.0132
SLL10-6 C	2.466	0.137	0.137	137.75	0.20	0.20	0.776	0.105	0.108	0.0887	0.0031	0.0030
SLL10-6 C	2.464	0.134	0.134	137.75	0.20	0.20	0.832	0.126	0.129	0.0910	0.0037	0.0031
SLL10-6 D re-cleaned	2.466	0.138	0.135	137.75	0.20	0.20	0.849	0.272	0.275	0.1385	0.0062	0.0055
SLL10-6 D re-cleaned	2.463	0.140	0.133	137.75	0.20	0.20	0.854	0.281	0.256	0.1371	0.0062	0.0051
SLL10-6 D-E hiatus	2.465	0.132	0.134	137.75	0.20	0.20	0.782	0.178	0.221	0.1198	0.0024	0.0024
SLL10-6 E	2.466	0.136	0.139	137.75	0.20	0.20	0.929	0.319	0.338	0.1640	0.0062	0.0056
SLL10-6 E	2.465	0.132	0.133	137.75	0.20	0.19	0.865	0.298	0.318	0.1604	0.0057	0.0053
SLL10-6 F top	2.466	0.132	0.143	137.75	0.20	0.20	0.960	0.047	0.054	0.0626	0.0013	0.0010
SLL10-6 F bottom	2.465	0.133	0.132	137.75	0.20	0.20	1.024	0.147	0.160	0.1143	0.0020	0.0022
SLL10-6 G	2.464	0.137	0.138	137.75	0.20	0.20	1.060	0.046	0.048	0.0572	0.0010	0.0010

Table 2c continued.

ID	ρ (^{238}U/^{206}Pb-^{207}Pb/^{206}Pb)[a]	ρ (^{234}U/^{206}Pb-^{207}Pb/^{206}Pb)[a]	ρ (^{207}Pb/^{206}Pb-^{208}Pb/^{206}Pb)[a]	% concord-ance (^{235}U-^{207}Pb age/^{238}U-^{206}Pb age)	+	-
SLL10-6 A	0.66	0.65	-0.08	-		
SLL10-6 A	0.42	0.42	-0.21	119.5	57.4	60.1
SLL10-6 B	0.50	0.50	0.05	-		
SLL10-6 B	0.49	0.49	-0.03	-		
SLL10-6 B re-cleaned	0.53	0.53	-0.20	-		
SLL10-6 B re-cleaned	-0.03	-0.03	0.15	116.3	53.1	54.0
SLL10-6 B-C hiatus	0.52	0.52	-0.19	-		
SLL10-6 C	0.58	0.58	0.30	99.9	13.8	14.4
SLL10-6 C	0.29	0.29	-0.09	106.6	16.3	16.6
SLL10-6 D re-cleaned	0.40	0.40	-0.09	98.5	31.8	32.0
SLL10-6 D re-cleaned	0.44	0.44	0.15	99.3	32.4	30.1
SLL10-6 D-E hiatus	0.69	0.69	0.12	90.7	20.6	25.4
SLL10-6 E	0.65	0.65	-0.34	107.4	37.3	39.3
SLL10-6 E	0.46	0.46	0.06	99.6	34.2	36.9
SLL10-6 F top	0.32	0.31	0.60	101.7	5.1	5.7
SLL10-6 F bottom	0.44	0.44	0.18	107.5	15.7	16.7
SLL10-6 G	0.59	0.59	0.06	98.5	4.5	4.6

Uncertainties are empirical 95% confidence Monte Carlo errors. The slight variations in the model values for different samples are random fluctuations arising from the Monte Carlo approach. Analyses with the same designation are replicate measurements of the same subsample.

[a]Correlation coefficient for the uncertainties on the specified ratio pairs.

[b]The assumed composition and uncertainty used to make corrections for the Pb initially in the samples.

495

Table 2d. U-Pb data obtained without precncentration of U and Pb, ^{238}U-^{206}Pb reference ages and ^{235}U-^{207}Pb ages for SB_PK_142. The ^{238}U-^{206}Pb reference ages use an arbitrary assumed initial ^{234}U/^{238}U and are included only to highlight the apparent age difference between the upper and lower portion of the sample.

ID	^{238}U/^{206}Pb	+	-	^{208}Pb/^{206}Pb	+	-	ρ (^{238}U/^{206}Pb-^{208}Pb/^{206}Pb)[a]	Model initial ^{234}U/^{238}U[c]	+	-
Subsamples 15-21 (stratigraphically younger than Fe stained lamina)										
SB_PK 142 (15)	630.5	14.3	14.2	0.6932	0.0186	0.0150	0.07	5.4999E-05	5.58E-08	5.37E-08
SB_PK 142 (15)	635.6	11.9	19.1	0.6912	0.0120	0.0113	0.19	5.5000E-05	5.38E-08	5.37E-08
SB_PK 142 (16)	726.7	8.4	10.3	0.4666	0.0276	0.0134	0.16	5.5000E-05	5.51E-08	5.53E-08
SB_PK 142 (16)	733.8	15.0	16.3	0.4535	0.0187	0.0150	0.10	5.5000E-05	5.66E-08	5.54E-08
SB_PK 142 (17)	753.5	17.4	21.3	0.4269	0.0274	0.0128	0.30	5.5000E-05	5.57E-08	5.30E-08
SB_PK 142 (17)	759.6	11.3	10.3	0.4118	0.0122	0.0091	0.25	5.5000E-05	5.42E-08	5.40E-08
SB_PK 142 (18)	851.3	6.7	6.5	0.0512	0.0009	0.0008	-0.17	5.5000E-05	5.60E-08	5.69E-08
SB_PK 142 (18)	860.5	14.7	13.4	0.0509	0.0010	0.0010	-0.11	5.5000E-05	5.41E-08	5.51E-08
SB_PK 142 (19)	897.4	16.3	16.1	0.0415	0.0007	0.0007	-0.06	5.5000E-05	5.54E-08	5.38E-08
SB_PK 142 (19)	917.2	16.0	15.7	0.0409	0.0010	0.0008	0.02	5.5000E-05	5.42E-08	5.50E-08
SB_PK 142 (20)	922.1	10.2	10.5	0.0167	0.0002	0.0003	0.03	5.5000E-05	5.65E-08	5.45E-08
SB_PK 142 (20)	906.5	10.9	10.8	0.0169	0.0003	0.0003	0.09	5.4999E-05	5.52E-08	5.47E-08
Subsamples 1-14 (stratigraphically older than Fe stained lamina)										
SB_PK 142 (1)	406.2	9.4	12.7	0.9789	0.0178	0.0165	0.07	5.5000E-05	5.46E-08	5.55E-08
SB_PK 142 (1)	404.8	9.1	9.0	0.9905	0.0223	0.0195	-0.05	5.5000E-05	5.50E-08	5.41E-08
SB_PK 142 (1)	399.1	9.8	9.4	0.9941	0.0277	0.0225	-0.05	5.5000E-05	5.56E-08	5.62E-08
SB_PK 142 (2)	677.8	18.2	18.0	0.0765	0.0049	0.0035	0.02	5.5001E-05	5.38E-08	5.45E-08
SB_PK 142 (2)	665.7	15.2	15.0	0.0720	0.0024	0.0021	0.04	5.5001E-05	5.38E-08	5.37E-08
SB_PK 142 (3)	656.2	14.4	13.9	0.0705	0.0017	0.0019	-0.14	5.5000E-05	5.55E-08	5.59E-08
SB_PK 142 (3)	664.4	11.2	10.9	0.0710	0.0013	0.0012	0.01	5.5000E-05	5.59E-08	5.53E-08
SB_PK 142 (4)	504.1	11.7	17.5	0.6115	0.0143	0.0143	-0.55	5.5000E-05	5.53E-08	5.43E-08
SB_PK 142 (4)	521.9	9.7	9.2	0.6011	0.0225	0.0113	0.31	5.5000E-05	5.50E-08	5.55E-08
SB_PK 142 (5)	695.3	5.7	6.5	0.0334	0.0011	0.0009	-0.35	5.5001E-05	5.34E-08	5.48E-08
SB_PK 142 (5)	665.5	9.0	8.5	0.0353	0.0007	0.0007	-0.13	5.5000E-05	5.63E-08	5.39E-08
SB_PK 142 (7)	652.0	16.3	15.8	0.0548	0.0017	0.0017	-0.06	5.4999E-05	5.47E-08	5.48E-08

500

Table 2d continued.

ID	Model com. ^{208}Pb/^{206}Pb[b]	+	-	^{238}U-^{206}Pb age (Ma) (assumed initial ^{234}U/^{238}U)[c]	+	-	^{235}U/^{207}Pb	+	-	^{208}Pb/^{207}Pb	+	-
Subsamples 15-21 (stratigraphically younger than Fe stained lamina)												
SB_PK 142 (15)	2.369	0.139	0.139	7.33	0.25	0.26	14.4	0.5	0.5	2.184	0.092	0.095
SB_PK 142 (15)	2.370	0.138	0.143	7.29	0.28	0.24	14.6	0.7	0.6	2.181	0.099	0.086
SB_PK 142 (16)	2.368	0.142	0.144	7.23	0.17	0.18	24.2	0.7	0.8	2.140	0.174	0.089
SB_PK 142 (16)	2.369	0.140	0.137	7.21	0.22	0.19	25.2	1.0	0.5	2.146	0.095	0.094
SB_PK 142 (17)	2.371	0.139	0.138	7.12	0.23	0.23	27.1	1.2	1.2	2.116	0.124	0.149
SB_PK 142 (17)	2.371	0.135	0.138	7.12	0.14	0.16	26.6	1.1	1.3	1.991	0.090	0.125
SB_PK 142 (18)	2.371	0.138	0.145	7.51	0.06	0.06	109.7	2.7	2.2	0.909	0.031	0.033
SB_PK 142 (18)	2.369	0.137	0.138	7.43	0.12	0.12	112.1	3.5	3.1	0.913	0.039	0.036
SB_PK 142 (19)	2.373	0.138	0.141	7.16	0.13	0.13	116.5	3.6	3.8	0.743	0.030	0.035
SB_PK 142 (19)	2.371	0.142	0.138	7.01	0.12	0.12	122.0	3.7	3.6	0.748	0.032	0.031
SB_PK 142 (20)	2.369	0.141	0.142	7.05	0.08	0.08	143.6	2.4	2.1	0.358	0.008	0.009
SB_PK 142 (20)	2.371	0.145	0.138	7.17	0.08	0.08	144.9	3.8	4.1	0.373	0.014	0.012
Subsamples 1-14 (stratigraphically older than Fe stained lamina)												
SB_PK 142 (1)	2.372	0.140	0.139	9.42	0.49	0.48	7.0	0.2	0.4	2.321	0.127	0.118
SB_PK 142 (1)	2.372	0.140	0.138	9.37	0.46	0.47	6.8	0.3	0.2	2.284	0.091	0.092
SB_PK 142 (1)	2.370	0.142	0.142	9.47	0.46	0.50	6.6	0.4	0.4	2.263	0.153	0.161
SB_PK 142 (2)	2.371	0.138	0.141	9.31	0.25	0.24	83.3	4.3	3.2	1.296	0.099	0.093
SB_PK 142 (2)	2.372	0.144	0.138	9.49	0.21	0.21	84.6	3.4	3.3	1.260	0.071	0.063
SB_PK 142 (3)	2.370	0.140	0.142	9.63	0.21	0.21	82.8	2.9	2.6	1.225	0.055	0.054
SB_PK 142 (3)	2.370	0.143	0.143	9.51	0.16	0.16	82.7	3.2	3.6	1.217	0.052	0.062
SB_PK 142 (4)	2.370	0.137	0.137	9.59	0.35	0.29	13.5	0.4	0.3	2.256	0.168	0.124
SB_PK 142 (4)	2.371	0.139	0.142	9.32	0.26	0.29	14.1	0.4	0.4	2.242	0.106	0.084
SB_PK 142 (5)	2.370	0.140	0.138	9.24	0.08	0.07	115.4	1.8	2.3	0.762	0.041	0.021
SB_PK 142 (5)	2.370	0.139	0.137	9.64	0.12	0.13	110.7	3.2	2.8	0.808	0.037	0.023
SB_PK 142 (7)	2.368	0.139	0.139	9.76	0.24	0.24	93.9	4.5	4.1	1.087	0.067	0.058

Table 2d continued.

ID	ρ (^{235}U/ ^{207}Pb- ^{208}Pb/ ^{207}Pb)[a]	Model com. ^{208}Pb/ ^{207}Pb[b]	+	-	Model ^{238}U/ ^{235}U	+	-	^{207}Pb- ^{235}U age (Ma)	+	-
Subsamples 15-21 (stratigraphically younger than Fe stained lamina)										
SB_PK 142 (15)	0.68	2.429	0.038	0.037	137.75	0.20	0.20	7.12	3.11	3.02
SB_PK 142 (15)	0.83	2.429	0.038	0.038	137.75	0.20	0.20	7.14	2.92	3.15
SB_PK 142 (16)	0.62	2.429	0.038	0.038	137.75	0.19	0.20	5.05	1.78	3.20
SB_PK 142 (16)	0.33	2.429	0.037	0.039	137.75	0.20	0.20	4.73	1.72	1.72
SB_PK 142 (17)	0.75	2.429	0.038	0.037	137.75	0.20	0.20	4.90	2.60	2.05
SB_PK 142 (17)	0.87	2.429	0.037	0.038	137.75	0.20	0.20	6.93	2.41	1.74
SB_PK 142 (18)	0.84	2.429	0.037	0.038	137.75	0.20	0.20	5.83	0.24	0.25
SB_PK 142 (18)	0.79	2.429	0.038	0.038	137.75	0.20	0.20	5.69	0.29	0.31
SB_PK 142 (19)	0.84	2.429	0.038	0.038	137.75	0.20	0.20	6.08	0.32	0.26
SB_PK 142 (19)	0.78	2.429	0.038	0.038	137.75	0.20	0.20	5.79	0.26	0.27
SB_PK 142 (20)	0.69	2.429	0.037	0.037	137.75	0.21	0.20	6.06	0.11	0.12
SB_PK 142 (20)	0.82	2.429	0.039	0.037	137.75	0.20	0.20	5.96	0.20	0.19
Subsamples 1-14 (stratigraphically older than Fe stained lamina)										
SB_PK 142 (1)	0.81	2.429	0.037	0.037	137.75	0.20	0.20			
SB_PK 142 (1)	0.66	2.429	0.038	0.038	137.75	0.20	0.19			
SB_PK 142 (1)	0.86	2.429	0.038	0.037	137.75	0.20	0.20			
SB_PK 142 (2)	0.51	2.429	0.038	0.037	137.75	0.20	0.20	5.72	0.63	0.68
SB_PK 142 (2)	0.70	2.429	0.039	0.038	137.75	0.21	0.19	5.81	0.51	0.51
SB_PK 142 (3)	0.61	2.429	0.037	0.038	137.75	0.21	0.20	6.11	0.44	0.44
SB_PK 142 (3)	0.85	2.429	0.038	0.038	137.75	0.20	0.20	6.16	0.59	0.47
SB_PK 142 (4)	0.66	2.429	0.037	0.038	137.75	0.21	0.20			
SB_PK 142 (4)	0.79	2.429	0.038	0.038	137.75	0.20	0.21			
SB_PK 142 (5)	0.62	2.429	0.037	0.039	137.75	0.20	0.20	6.07	0.19	0.24
SB_PK 142 (5)	0.71	2.429	0.037	0.038	137.75	0.21	0.20	6.15	0.22	0.31
SB_PK 142 (7)	0.71	2.429	0.037	0.037	137.75	0.20	0.20	6.01	0.50	0.53

505

Table 2d continued.

ID	^{207}Pb/ ^{206}Pb	+	-	Initial (^{234}U/ ^{238}U)	+	-
Subsamples 15-21 (stratigraphically younger than Fe stained lamina)						
SB_PK 142 (15)	0.3175	0.0120	0.0127	1.6	8.7	8.8
SB_PK 142 (15)	0.3170	0.0098	0.0139	1.4	8.9	8.2
SB_PK 142 (16)	0.2181	0.0060	0.0059	7.2	8.8	5.1
SB_PK 142 (16)	0.2114	0.0063	0.0083	8.0	4.9	5.0
SB_PK 142 (17)	0.2022	0.0117	0.0123	7.3	6.3	7.4
SB_PK 142 (17)	0.2071	0.0102	0.0091	1.5	5.0	6.7
SB_PK 142 (18)	0.0564	0.0013	0.0015	5.8	0.7	0.7
SB_PK 142 (18)	0.0557	0.0018	0.0019	5.9	1.0	0.9
SB_PK 142 (19)	0.0559	0.0022	0.0020	4.1	0.9	1.0
SB_PK 142 (19)	0.0546	0.0019	0.0019	4.4	0.9	0.9
SB_PK 142 (20)	0.0466	0.0008	0.0008	3.8	0.4	0.4
SB_PK 142 (20)	0.0454	0.0013	0.0012	4.4	0.5	0.6
Subsamples 1-14 (stratigraphically older than Fe stained lamina)						
SB_PK 142 (1)	0.4219	0.0272	0.0218			
SB_PK 142 (1)	0.4339	0.0155	0.0180			
SB_PK 142 (1)	0.4399	0.0292	0.0292			
SB_PK 142 (2)	0.0591	0.0028	0.0032	11.1	2.2	2.1
SB_PK 142 (2)	0.0572	0.0026	0.0024	11.4	1.7	1.7
SB_PK 142 (3)	0.0576	0.0021	0.0020	10.9	1.4	1.5
SB_PK 142 (3)	0.0583	0.0027	0.0022	10.5	1.4	1.7
SB_PK 142 (4)	0.2712	0.0101	0.0146			
SB_PK 142 (4)	0.2682	0.0089	0.0083			
SB_PK 142 (5)	0.0438	0.0010	0.0010	10.0	0.9	0.6
SB_PK 142 (5)	0.0436	0.0011	0.0013	10.9	0.9	0.7
SB_PK 142 (7)	0.0504	0.0027	0.0026	11.6	1.8	1.8

Uncertainties are empirical 95% confidence Monte Carlo errors. The slight variations in the model values for different samples are random fluctuations arising from the Monte Carlo approach. Analyses with the same designation are replicate measurements of the same subsample.

[a]Correlation coefficient for the uncertainties on the specified ratio pairs.
[b]The assumed composition and uncertainty used to make corrections for the Pb initially in the samples.
[c]The initial ^{234}U/^{238}U ratio is arbitrarily chosen to allow ^{238}U/^{206}Pb ages to be calculated to show the apparent age differences between the different sections of SB_PK 142. The ^{238}U/^{206}Pb ages should not be taken as an accurate estimate of the true age.
[d]The estimated initial ^{234}U/^{238}U ratio estimated from the ^{238}U/radiogenic^{206}Pb ratio using the ^{235}U-^{207}Pb age.

Table 2e. U-Pb data and ^{238}U-^{206}Pb reference ages for JOHO-1 obtained without preconcentration of U and Pb.

510

ID	^{238}U/ ^{206}Pb	+	-	^{208}Pb/ ^{206}Pb	+	-	^{207}Pb/ ^{206}Pb	+	-	Model initial ^{234}U/ ^{238}U[c]	+	-
JOHO-1 311.0 (1)	294.6	5.2	7.2	0.1455	0.0046	0.0069	0.1013	0.0104	0.0064	5.50E-05	5.60E-06	5.17E-06
JOHO-1 311.0 (1)	307.0	6.9	7.0	0.1450	0.0082	0.0051	0.0992	0.0178	0.0066	5.51E-05	5.45E-06	5.55E-06
JOHO-1 311.0 (1)	297.0	7.0	6.1	0.1537	0.0143	0.0093	0.1495	0.4652	0.0557	5.50E-05	5.18E-06	5.30E-06
JOHO-1 311.0 (2)	321.6	5.5	6.2	0.0713	0.0231	0.0093	0.0801	0.0204	0.0074	5.49E-05	5.53E-06	5.66E-06
JOHO-1 311.0 (2)	325.2	8.9	7.2	0.0867	0.0317	0.0123	0.0664	0.0029	0.0027	5.51E-05	5.25E-06	5.68E-06
JOHO-1 311.0 (2)	324.3	4.0	4.3	0.0613	0.0069	0.0036	0.0701	0.0054	0.0044	5.49E-05	5.19E-06	5.60E-06
JOHO-1 311.0 (3)	328.9	15.1	7.2	0.0495	0.0028	0.0021	0.0640	0.0035	0.0037	5.50E-05	5.89E-06	5.62E-06
JOHO-1 311.0 (3)	321.8	7.0	8.2	0.0498	0.0027	0.0033	0.0647	0.0036	0.0027	5.51E-05	5.50E-06	5.13E-06
JOHO-1 311.0 (3)	320.8	5.3	5.0	0.0486	0.0020	0.0020	0.0626	0.0039	0.0026	5.49E-05	5.41E-06	5.05E-06
JOHO-1 311.0 (4)	338.0	9.9	9.5	0.0889	0.0050	0.0048	0.0874	0.0648	0.0096	5.52E-05	5.25E-06	5.21E-06
JOHO-1 311.0 (4)	324.3	9.8	18.5	0.0986	0.0055	0.0066	0.0816	0.0048	0.0068	5.50E-05	5.01E-06	4.78E-06
JOHO-1 311.0 (4)	317.0	8.8	8.7	0.0924	0.0096	0.0048	0.0764	0.0050	0.0038	5.50E-05	5.64E-06	5.35E-06

515   Table 2e continued.

ID	Model com. ^{208}Pb/^{206}Pb[b]	+	-	^{238}U-^{206}Pb age (Ma) (assumed initial ^{234}U/^{238}U)[c]	+	-	ρ (^{238}U/^{206}Pb-^{208}Pb/^{206}Pb)[a]
JOHO-1 311.0 (1)	2.20	0.53	0.49	20.50	0.56	0.54	-0.18
JOHO-1 311.0 (1)	2.20	0.50	0.48	19.68	0.54	0.59	0.21
JOHO-1 311.0 (1)	2.20	0.46	0.51	20.25	0.54	0.67	0.14
JOHO-1 311.0 (2)	2.19	0.49	0.49	19.46	0.39	0.42	-0.22
JOHO-1 311.0 (2)	2.20	0.48	0.48	19.11	0.51	0.57	-0.11
JOHO-1 311.0 (2)	2.20	0.48	0.53	19.40	0.30	0.28	-0.19
JOHO-1 311.0 (3)	2.20	0.49	0.51	19.23	0.44	0.86	-0.23
JOHO-1 311.0 (3)	2.18	0.50	0.54	19.65	0.50	0.44	-0.01
JOHO-1 311.0 (3)	2.21	0.50	0.48	19.73	0.35	0.35	0.29
JOHO-1 311.0 (4)	2.22	0.47	0.50	18.38	0.54	0.53	-0.35
JOHO-1 311.0 (4)	2.20	0.52	0.52	19.06	1.15	0.65	-0.17
JOHO-1 311.0 (4)	2.20	0.49	0.52	19.55	0.57	0.56	0.01

Uncertainties are empirical 95% confidence Monte Carlo errors. The slight variations in the model values for different samples are random fluctuations arising from the Monte Carlo approach.

[a]Correlation coefficient for the uncertainties on the specified ratio pairs.

[b]The assumed composition and uncertainty used to make corrections for the Pb initially in the samples.

[c]The initial ^{234}U/^{238}U ratio is arbitrarily chosen to allow ^{238}U/^{206}Pb ages to be calculated. In the absence of direct constraint of the initial ^{234}U/^{238}U ratio, these ages should be treated with caution.

Table 2f. Reference laser ablation U-Pb data for JOHO-1.

Spot	^{238}U/^{206}Pb	+/-	^{207}Pb/^{206}Pb	+/-
JOHO-1_01	211.8	16.0	0.3043	0.0387
JOHO-1_02	202.8	16.4	0.2791	0.0328
JOHO-1_03	317.3	8.1	0.0682	0.0032
JOHO-1_04	274.9	8.6	0.1396	0.0111
JOHO-1_05	283.2	10.6	0.1350	0.0108
JOHO-1_06	319.6	12.0	0.0796	0.0059
JOHO-1_07	311.4	10.1	0.0724	0.0059
JOHO-1_08	283.9	13.6	0.1450	0.0183
JOHO-1_09	275.1	7.8	0.1542	0.0068
JOHO-1_10	301.6	11.8	0.1713	0.0094
JOHO-1_11	331.7	8.2	0.0505	0.0016
JOHO-1_12	333.1	8.2	0.0578	0.0019
JOHO-1_13	325.0	8.3	0.0549	0.0016
JOHO-1_14	284.8	10.8	0.1481	0.0118
JOHO-1_15	309.1	12.2	0.1183	0.0082
JOHO-1_16	318.1	9.9	0.0693	0.0041
JOHO-1_17	319.6	8.6	0.0716	0.0038
JOHO-1_18	316.7	9.6	0.0692	0.0039
JOHO-1_19	256.6	11.1	0.1828	0.0125
JOHO-1_20	275.2	11.2	0.1508	0.0113
JOHO-1_21	333.0	8.4	0.0592	0.0032
JOHO-1_22	338.4	7.4	0.0496	0.0014
JOHO-1_23	305.6	8.9	0.0987	0.0061
JOHO-1_24	322.6	8.5	0.0751	0.0042
JOHO-1_25	319.5	9.1	0.0796	0.0055
JOHO-1_26	309.9	8.8	0.0826	0.0059
JOHO-1_27	306.4	7.9	0.1006	0.0060
JOHO-1_28	293.3	8.9	0.1173	0.0094
JOHO-1_29	326.5	8.5	0.0542	0.0018
JOHO-1_30	296.8	10.5	0.1150	0.0082
JOHO-1_31	297.2	12.6	0.1032	0.0150
JOHO-1_32	310.5	8.3	0.0767	0.0031
JOHO-1_33	327.4	8.8	0.0574	0.0020
JOHO-1_34	340.3	8.0	0.0531	0.0017
JOHO-1_35	322.8	10.0	0.0800	0.0051
JOHO-1_36	328.5	8.9	0.0594	0.0023
JOHO-1_37	317.6	9.1	0.0803	0.0036
JOHO-1_38	319.5	8.5	0.0803	0.0046
JOHO-1_39	338.5	8.3	0.0566	0.0019
JOHO-1_40	302.1	9.8	0.0983	0.0058
JOHO-1_41	68.6	15.4	0.5229	0.0385
JOHO-1_42	318.3	9.5	0.0698	0.0037
JOHO-1_43	320.2	7.6	0.0627	0.0023
JOHO-1_44	238.5	22.8	0.2137	0.0424
JOHO-1_45	197.2	11.6	0.3376	0.0291
JOHO-1_46	336.6	8.4	0.0643	0.0036
JOHO-1_47	335.6	8.3	0.0497	0.0020
JOHO-1_48	332.5	8.0	0.0587	0.0027
JOHO-1_49	346.5	8.3	0.0513	0.0016
JOHO-1_50	334.3	8.7	0.0637	0.0035
JOHO-1_51	250.6	11.3	0.2200	0.0188
JOHO-1_52	330.4	8.5	0.0678	0.0032
JOHO-1_53	338.3	9.0	0.0754	0.0050
JOHO-1_54	319.7	9.0	0.0809	0.0037
JOHO-1_55	306.3	8.9	0.1270	0.0050
JOHO-1_56	339.3	8.9	0.0688	0.0026
JOHO-1_57	340.6	8.6	0.0487	0.0016
JOHO-1_58	338.5	8.8	0.0526	0.0017
JOHO-1_59	333.3	8.0	0.0645	0.0052
JOHO-1_60	322.3	8.6	0.0606	0.0027

Uncertainties are 2 sigma

520

7 Discussion

525 ### 7.1 Method validation

The results from the samples used for method validation indicate that the new protocol passes the four method validation tests.

Not separating the matrix does not lead to an inconsistency of data in the preliminary test using ASH-15, that is to say the
530 data with and without matrix separation are co-linear, i.e. they define a common isochron and therefore would yield the same
^{238}U/^{206}Pb age. Replication of ^{238}U-^{234}U-^{206}Pb ages with and without matrix separation is demonstrated to a high-precision
for the F and G layers of SLL10-6, again demonstrating that matrix separation via anion exchange chemistry is not necessary
for the U/Pb measurements. This finding is in line with the fact that laser ablation techniques have been making
measurements for a number of years without matrix separation (e.g. Roberts et al., 2017).

535

For SLL10-6, ^{238}U-^{234}U-^{206}Pb ages obtained with the new protocol from all stratigraphic layers vary systematically with
stratigraphic order, with no age reversals. Moreover, for sample layers that are sufficiently radiogenic to allow ^{235}U-^{207}Pb
ages to be calculated, these are concordant with the ^{238}U-^{234}U-^{206}Pb ages, demonstrating the ability of the new protocol to
exploit the ^{235}U-^{207}Pb system where the nature of the sample permits, even on material as young as c. 1 Ma. This is
540 significant because it demonstrates the ability to have a continuity of dating between young samples where the initial ^{234}U
can be directly constrained via the ^{238}U-^{234}U-^{206}Pb chronometer and old material (i.e. >20 Ma) where ^{238}U-^{206}Pb age
inaccuracies associated with assuming the initial ^{234}U/^{238}U ratio will be proportionally small compared to the age.

Analysis of JOHO-1 using the new protocol replicates independently obtained laser ablation data demonstrating inter-
545 laboratory consistency of the new method. Additional data quality tests of the new method are presented in the larger data set
of Vaks et al., (2020) in the form of comparison with U-Th ages and the testing of age reproducibility between different
speleothems from a single location.

7.2 ^{238}U-^{206}Pb Russian roulette and the utility of the ^{235}U-^{207}Pb system

One of the major limitation to applying the ^{238}U-^{206}Pb system to geologically young materials just beyond the limit of the
550 ^{238}U-^{234}U-^{206}Pb chronometer (a few million years) is that while ages can be highly precise (e.g. Woodhead et al., 2006), an
age calculated assuming equilibrium initial ^{234}U/^{238}U and one calculated using the most extreme known initial ^{234}U/^{238}U ratio

differ by >2 Ma, which is proportionally a massive difference for ages of a few million years. While is it possible to try to characterise initial $^{234}U/^{238}U$ for a particular cave using younger material (e.g. Woodhead et al., 2006), it is difficult to test whether such younger material is representative, and in some instances, younger material may simply not exist.

555 Consequently, ^{238}U-^{206}Pb dating beyond the limit of the ^{238}U-^{234}U-^{206}Pb chronometer is something of a game of Russian roulette in terms of age accuracy, with SB_pk142 from Botovskaya cave being an example of where the 'bullet' of extreme initial ^{234}U disequilibrium is in the chamber. The ^{235}U-^{207}Pb chronometer provides an alternative option for highly radiogenic samples. Moreover, because decay of excess ^{234}U leads to a permanent excess of radiogenic ^{206}Pb relative to radiogenic ^{207}Pb, comparison of the ^{238}U-^{206}Pb and ^{235}U-^{207}Pb systems can be used to constrain initial $^{234}U/^{238}U$ after any residual

560 disequilibrium has decayed (e.g. Mason et al., 2013). This is potentially very useful for testing assumed initial $^{238}U/^{234}U$ ratios used for other samples in a set where these can only be dated by the ^{238}U-^{206}Pb chronometer, because of common Pb.

7.3 Applicability of the new protocol and potential future development

The present method is only applicable to samples in which ^{232}Th is near absent. The method is not intended as a blanket

565 replacement for prior implementations of the U-Pb system, but rather as a complementary technique that can be applied where it is best suited. Traditional solution based methods, for example, are clearly always likely to be the preferred approach for the calibration of reference materials (e.g. Roberts et al., 2017), and *in situ* techniques are still needed where high spatial resolution is required on samples that are very small or have a complex morphology (e.g. Li et al., 2014). Nevertheless, the minimal sample preparation, elimination of separate U/Pb reconnaissance, and minimisation of the use of

570 isochrons in favour of model ages makes the new method a useful addition. The utilisation of the new approach by us (Vaks et al., 2020) to obtain c. 50 ^{238}U-^{234}U-^{206}Pb ages, many with corresponding concordant ^{235}U-^{207}Pb ages, on material <1.6 Ma old, demonstrates that it can be applied effectively 'in the wild' to generate fairly large data sets. Indeed, the reduction in analytical effort achieved allowed replication of growth ages between different stalagmites, providing additional quality control that would not otherwise have been available. The results from JOHO-1 indicate the method can be applied to

575 carbonates with <1 ppm U.

Demonstrating the ability to make U-Pb measurements by directly dissolving samples with an isotopic tracer, and analysing with no further preparation other that dilution, opens an intriguing possibility for future method development; the prospect of some form of quasi-*in situ* isotope dilution analysis. If an acid cleaned subsample can be dissolved directly with the tracer

580 and analysed, there is no reason, in principle, why an entire sample could not be acid cleaned, and small domains then dissolved with the tracer for analysis while still *in situ*. Obviously, there would be practical hurdles to overcome, and this would not be a substitute for high spatial resolution techniques, but it could substantially streamline isotope dilution analysis and make it less destructive to the sample.

8 Conclusions

585 A new isotope dilution based method for the U-Pb dating of carbonate samples is presented which removes the need for labour-intensive preconcentration of Pb. The new method produces data consistent with those obtained by isotope dilution with preconcentration of U and Pb, and with data obtained independently by another laboratory using laser ablation ICP-MS. The new method also generates self-consistent data, specifically, ages that vary systematically with growth direction without age reversals and which are concordant between the ^{238}U-^{234}U-^{206}Pb and the ^{235}U-^{207}Pb chronometers. The new method thus

590 satisfies reasonable data quality control criteria.

The new method is capable of utilising both the ^{238}U-^{234}U-^{206}Pb chronometer and the ^{235}U-^{207}Pb chronometers, subject to inherent limitations imposed by sample age and isotopic composition.

595 **Data Availability.** All data used are contained within Table 2.

Author Contribution. AV obtained funding partially supporting this work. AV, SB and JH obtained samples and assisted with sample preparation. AM carried out the isotope dilution method development, analyses, and age interpretation. JH provided reference laser ablation data. AM wrote the manuscript with input from all co-authors.

600

Competing interests. The authors declare that they have no conflict of interest.

Acknowledgements. NERC grants NE/K005057/1 and NE/G013829/1 and DFG grant BR 3437/3-1 are acknowledged for partially supporting the present work. Speleoclub Arabika Irkutsk is thanked for invaluable assistance in obtaining

605 speleothem samples from Siberia. Dr Nick Roberts (NIGL) is thanked for assistance in obtaining reference laser ablation data for JOHO-1. Shell is thanked for providing sample JOHO-1.

References

Bajo, P., Drysdale, R., Woodhead, J., Hellstrom, J. and Zanchetta, G.: High-resolution U-Pb dating of an Early Pleistocene stalagmite from Corchia Cave (central Italy), Quat. Geochronol., 14, 5–17, doi:10.1016/j.quageo.2012.10.005, 2012.

610 Belshaw, N. S., Freedman, P. A., O'Nions, R. K., Frank, M. and Guo, Y.: A new variable dispersion double-focusing plasma mass spectrometer with performance illustrated for Pb isotopes, Int. J. Mass Spectrom., 181, 51–58, 1998.

Cheng, H., Edwards, R. L., Murrell, M. T. and Benjamin, T. M.: Uranium-thorium-protactinium dating systematics, Geochim. Cosmochim. Acta, 62(21–22), 3437–3452, doi:10.1016/S0016-7037(98)00255-5, 1998.

Cheng, H., Lawrence Edwards, R., Shen, C. C., Polyak, V. J., Asmerom, Y., Woodhead, J., Hellstrom, J., Wang, Y., Kong,
615   X., Spötl, C., Wang, X. and Calvin Alexander, E.: Improvements in ^{230}Th dating, ^{230}Th and ^{234}U half-life values, and U-Th
isotopic measurements by multi-collector inductively coupled plasma mass spectrometry, Earth Planet. Sci. Lett., 371–372,
82–91, doi:10.1016/j.epsl.2013.04.006, 2013.

Cliff, R. A., Spötl, C. and Mangini, A.: U-Pb dating of speleothems from Spannagel Cave, Austrian Alps: A high resolution
comparison with U-series ages, Quat. Geochronol., 5(4), 452–458, doi:10.1016/j.quageo.2009.12.002, 2010.

620   Edwards, R. L., Gallup, C. D. and Cheng, H.: Uranium-series Dating of Marine and Lacustrine Carbonates, Rev. Mineral.
Geochemistry, 52(1), 363–405, doi:10.2113/0520363, 2003.

Faure, G.: Principles of Isotope Geology, John Wiley & Sons, New York, 1986.

Getty, S. R., Asmerom, Y., Quinn, T. M. and Budd, A. F.: Accelerated Pleistocene coral extinctions in the Caribbean Basin
shown   by   uranium-lead   (U-Pb)   dating,   Geology,   29(7),   639–642,   doi:10.1130/0091-
625   7613(2001)029<0639:APCEIT>2.0.CO;2, 2001.

Heaman, L. and Parrish, R.: U-Pb Geochrononology of Accessory Minerals, in Short course Handbook on Applications of
Radiogenic Isotope Systems to Problems in Geology, edited by L. Heaman and J. N. Ludden, pp. 59–102, Mineralogical
Association of Canada., 1991.

Hiess, J., Condon, D. J., McLean, N. and Noble, S. R.: ^{238}U/^{235}U Systematics in Terrestrial Uranium-Bearing Minerals,
630   Science, 335(6076), 1610 LP – 1614, doi:10.1126/science.1215507, 2012.

Kronfeld, J., Vogel, J. C. and Talma, A. S.: A new explanation for extreme ^{234}U/^{238}U disequilibria in a dolomitic aquifer,
Earth Planet. Sci. Lett., 123(1–3), 81–93, doi:10.1016/0012-821X(94)90259-3, 1994.

Li, Q., Parrish, R. R., Horstwood, M. S. A. and Mcarthur, J. M.: U – Pb dating of cements in Mesozoic ammonites, Chem.
Geol., 376, 76–83, doi:10.1016/j.chemgeo.2014.03.020, 2014.

635   Lin, Y., Jochum, K. P., Scholz, D., Hoffmann, D. L., Stoll, B., Weis, U. and Andreae, M. O.: In-situ high spatial resolution
LA-MC-ICPMS 230Th/U dating enables detection of small-scale age inversions in speleothems, Solid Earth Sci., 2(1), 1–9,
doi:10.1016/j.sesci.2016.12.003, 2017.

Ludwig, K. R.: Effect of initial radioactive-daughter disequilibrium on U-Pb isotope apparent ages of young minerals, J.
Res., 5(6), 663–667, 1977.

640   Mason, A. J. and Henderson, G. M.: Correction of multi-collector-ICP-MS instrumental biases in high-precision uranium-
thorium chronology, Int. J. Mass Spectrom., 295(1–2), 26–35, doi:10.1016/j.ijms.2010.06.016, 2010.

Mason, A. J., Henderson, G. M. and Vaks, A.: An acetic acid-based extraction protocol for the recovery of U, Th and Pb
from calcium carbonates for U-(Th)-Pb geochronology, Geostand. Geoanalytical Res., 37(3), 261–275, doi:10.1111/j.1751-
908X.2013.00219.x, 2013.

645   Moorbath, S., Taylor, P. N., Orpen, J. L., Treloar, P. and Wilson, J. F.: First direct radiometric dating of Archaean
stromatolitic limestone, Nature, 326(6116), 865–867, doi:10.1038/326865a0, 1987.

Nuriel, P., Rosenbaum, G., Zhao, J.-X., Feng, Y., Golding, S. D., Villemant, B. and Weinberger, R.: U-Th dating of striated fault planes, Geology, 40(7), 647–650, doi:10.1130/G32970.1, 2012.

Pickering, R., Kramers, J. D., Partridge, T., Kodolanyi, J. and Pettke, T.: Quaternary Geochronology U – Pb dating of calcite

650 – aragonite layers in speleothems from hominin sites in South Africa by MC-ICP-MS, Quat. Geochronol., 5(5), 544–558, doi:10.1016/j.quageo.2009.12.004, 2010.

Plagnes, V., Causse, C., Genty, D., Paterne, M. and Blamart, D.: A discontinuous climatic record from 187 to 74 ka from a speleothem of the Clamouse Cave (south of France), Earth Planet. Sci. Lett., 201(1), 87–103, doi:10.1016/S0012-821X(02)00674-X, 2002.

655 Rasbury, E. T. and Cole, J. M.: Directly dating geologic events: U-Pb dating of carbonates, Rev. Geophys., 47, 1–27, doi:10.1029/2007RG000246.1.INTRODUCTION, 2009.

Rasbury, E. T., Hanson, G. N., Meyers, W. J. and Saller, A. H.: Dating of the time of sedimentation using U□Pb ages for paleosol calcite, Geochim. Cosmochim. Acta, 61(7), 1525–1529, doi:https://doi.org/10.1016/S0016-7037(97)00043-4, 1997.

Richards, D. A., Bottrell, S. H., Cliff, R. A., Ströhle, K. and Rowe, P. J.: U-Pb dating of a speleothem of Quaternary age,

660 Geochim. Cosmochim. Acta, 62(23), 3683–3688, 1998.

Roberts, N. M. W., Rasbury, E. T., Parrish, R. R., Smith, C. J., Horstwood, M. S. A. and Condon, D. J.: A calcite reference material for LA-ICP-MS U-Pb geochronology, Geochemistry, Geophys. Geosystems, 2807–2814, doi:10.1002/2016GC006784.Received, 2017.

Scholz, D. and Hoffmann, D.: 230Th/U-dating of fossil corals and speleothems, E&G Quat. Sci. J., 57(1/2), 52–76,

665 doi:10.3285/eg.57.1-2.3, 2008.

Spooner, P. T., Chen, T., Robinson, L. F. and Coath, C. D.: Rapid uranium-series age screening of carbonates by laser ablation mass spectrometry, Quat. Geochronol., 31, 28–39, doi:10.1016/j.quageo.2015.10.004, 2016.

Steiger, R. H. and Jäger, E.: Subcommission on geochronology: Convention on the use of decay constants in Geo- and Cosmochronology, Earth Planet. Sci. Lett., 36, 359–362, 1977.

670 Thomas, A. L., Fujita, K., Iryu, Y., Bard, E., Cabioch, G., Camoin, G., Cole, J. E., Deschamps, P., Durand, N., Hamelin, B., Heindel, K., Henderson, G. M., Mason, A. J., Matsuda, H., Ménabréaz, L., Omori, A., Quinn, T., Sakai, S., Sato, T., Sugihara, K., Takahashi, Y., Thouveny, N., Tudhope, A. W., Webster, J., Westphal, H. and Yokoyama, Y.: Assessing subsidence rates and paleo water-depths for Tahiti reefs using U-Th chronology of altered corals, Mar. Geol., 295–298, 86–94, doi:10.1016/j.margeo.2011.12.006, 2012.

675 Vaks, A., Woodhead, J., Bar-matthews, M., Ayalon, A., Cliff, R. A. and Zilberman, T.: Pliocene – Pleistocene climate of the northern margin of Saharan – Arabian Desert recorded in speleothems from the Negev Desert , Israel, Earth Planet. Sci. Lett., 368, 88–100, doi:10.1016/j.epsl.2013.02.027, 2013a.

Vaks, A., Gutareva, O. S., Breitenbach, S. F. M., Avirmed, E., Mason, A. J., Thomas, A. L., Osinzev, A. V, Kononov, A. M. and Henderson, G. M.: Speleothems reveal 500,000-year history of Siberian permafrost., Science (80-.)., 61(21), 183–186

680   [online] Available from: http://www.ncbi.nlm.nih.gov/pubmed/23429705, 2013b.

Vaks, A., Mason, A. J., Breitenbach, S. F. M., Kononov, A. M., Osinzev, A. V., Rosensaft, M., Borshevsky, A., Gutareva, O. S. and Henderson, G. M.: Palaeoclimate evidence of vulnerable permafrost during times of low sea ice, Nature, 577(7789), 221–225, doi:10.1038/s41586-019-1880-1, 2020.

Wang, Z. S., Rasbury, E. T., Hanson, G. N. and Meyers, W. J.: Using the U-Pb system of calcretes to date the time of

685   sedimentation of clastic sedimentary rocks, Geochim. Cosmochim. Acta, 62(16), 2823–2835, doi:https://doi.org/10.1016/S0016-7037(98)00201-4, 1998.

Woodhead, J. and Petrus, J.: Exploring the advantages and limitations of in situ U–Pb carbonate geochronology using speleothems, Geochronology, 1(1), 69–84, doi:10.5194/gchron-1-69-2019, 2019.

Woodhead, J. and Pickering, R.: Beyond 500 ka : Progress and prospects in the U \ Pb chronology of speleothems , and their

690   application to studies in palaeoclimate , human evolution , biodiversity and tectonics, Chem. Geol., 322–323, 290–299, doi:10.1016/j.chemgeo.2012.06.017, 2012.

Woodhead, J., Hellstrom, J., Maas, R., Drysdale, R., Zanchetta, G., Devine, P. and Taylor, E.: U – Pb geochronology of speleothems by MC-ICPMS, Quat. Geochronol., 1, 208–221, doi:10.1016/j.quageo.2006.08.002, 2006.

York, D.: Least squares fitting of a straight line with correlated errors, Earth Planet. Sci. Lett., 5(Xi), 320–324, 1969.

695